haematologica
Journal of the Ferrata Storti Foundation

Bleximenib, the novel menin-KMT2A inhibitor JNJ-75276617, impairs long-term proliferation and immune evasion in acute myeloid leukemia

by Shanna M. Hogeling, Duy Minh Lê, Nikita La Rose, Min Chul Kwon, Albertus T.J. Wierenga, Fiona A.J. van den Heuvel, Vincent van den Boom, Anna Kuchnio, Ulrike Philippar, Gerwin Huls and Jan Jacob Schuringa

Received: April 16, 2024.
Accepted: December 13, 2024.

Citation: Shanna M. Hogeling, Duy Minh Lê, Nikita La Rose, Min Chul Kwon, Albertus T.J. Wierenga, Fiona A.J. van den Heuvel, Vincent van den Boom, Anna Kuchnio, Ulrike Philippar, Gerwin Huls and Jan Jacob Schuringa. Bleximenib, the novel menin-KMT2A inhibitor JNJ-75276617, impairs long-term proliferation and immune evasion in acute myeloid leukemia. Haematologica. 2024 Dec 19. doi: 10.3324/haematol.2024.285616 [Epub ahead of print]

Bleximenib, the novel menin-KMT2A inhibitor JNJ-75276617, impairs long-term proliferation and immune evasion in acute myeloid leukemia

Shanna M. Hogeling[1], Duy Minh Lê[1], Nikita La Rose[1], Min Chul Kwon[2], Albertus T.J. Wierenga[1], Fiona A.J. van den Heuvel[1], Vincent van den Boom[1], Anna Kuchnio[2], Ulrike Philippar[2], Gerwin Huls[1] and Jan Jacob Schuringa[1*]

[1]Department of Hematology, University Medical Center Groningen, University of Groningen, Groningen, The Netherlands; [2]Discovery Oncology, Janssen R&D, Beerse, Belgium.

Running head: The novel menin-KMT2A inhibitor JNJ-75276617

[*]corresponding author:

Prof.dr. J.J. Schuringa, PhD

Department of Experimental Hematology

University Medical Center Groningen

Hanzeplein 1, PO Box 30.001, 9700 RB Groningen, The Netherlands

Phone: + 31503612354, Fax: +31503615960

E-mail: j.j.schuringa@umcg.nl

Data and materials availability All data are available in the main text or the supplementary materials. ChIP-sequencing data can be found at GSE237834 and proteome data at PXD030487.

Funding

This work was supported by a grant from the Dutch Cancer Foundation to JJS (11013) and a PPP grant from Health Holland/TKI (LSHM200204)

Author contributions

SMH, DML, NLR, ATJW, FAJvdH, VvdB, JJS performed research. SMH, DML, NLR, MCK, ATJW, FAJvdH, VvdB, AK, UP, GH and JJS discussed and analyzed data. MCK, AK, and UP provided compounds. SMH and JJS wrote the manuscript, which was edited and approved by all authors.

Competing interests: MCK, AK, and UP are currently employees of Janssen Research & Development and may own stock/stock options in Johnson & Johnson. The other authors disclose no conflicts of interest.

Abstract

Acute myeloid leukemia (AML) remains challenging to treat, which in part relates to genetic heterogeneity of the disease, to the protective tumor microenvironment driving resistance to therapy, and also to immune evasion characteristics of leukemic cells. Targeting epigenetic programs in AML provides an attractive opportunity to impair long-term proliferation and induce differentiation. The novel inhibitor JNJ-75276617 (bleximenib) targets the menin-KMT2A interaction and provides preclinical efficacy in AML (Kwon *et al*[1]). Here, we provide mechanistic insight in how JNJ-75276617 impairs proliferation and drives differentiation of primary AML patient cells. A large-scale drug screen was set up in which genetic alterations and quantitative proteomics were compared with drug sensitivity in a preclinical setting, which revealed that granulocyte macrophage progenitor (GMP)-like AMLs display the greatest sensitivity. Furthermore, we identified that *NPM1c*/*DNMT3A*^{mut} AMLs are sensitive, and some *NPM1*^{wt} AML subtypes without *KMT2A*-*MLLT3* rearrangements benefit from menin-KMT2A inhibition. Genome-wide ChIP-seq studies revealed patient-specific epigenetic alterations upon JNJ-75276617 treatment, uncovering a striking upregulation of MHC class I and class II expression as a consequence of epigenetic changes upon menin-KMT2A inhibition, independent of MEIS1 loss but involving CIITA activation. Functionally, this results in enhanced sensitivity of leukemic blasts to T cell-mediated cytotoxicity in allogeneic and autologous settings. Our data indicate that JNJ-75276617 provides a potential therapeutic approach whereby not only proliferation is impaired and differentiation is induced, but whereby therapeutic benefit might also be achieved by reactivating the antigen presentation machinery.

Introduction

Acute myeloid leukemia (AML) is a heterogeneous disease initiated by genetic mutations, whereby a block in differentiation leads to accumulation of hematopoietic stem and progenitor cells in the bone marrow.[2] Curative treatment has remained challenging, in part related to the complexity of the disease whereby multiple genetically distinct sub-clones frequently co-occur within individual patients, further complicating treatment efficacy.[3,4] While the usual backbone of treatment entails '7+3' chemotherapy consisting of anthracyclines and cytarabine, new targeted therapies are emerging. For instance, specific inhibitors against *FLT3*, BCL2*, JAK2*, *IDH1* and *IDH2* mutations have now been added to treatment options for AML depending on mutational status and fitness of the patient. For patients with *KMT2A* (lysine methyltransferase 2A; previously mixed-lineage leukemia (*MLL*)) rearrangements and *NPM1* (Nucleophosmin 1) mutations there are no FDA-approved targeted therapies available thus far.

The *KMT2A* gene is a member of the Trithorax group, which includes, among others, 3 pairs of family members *KMT2A/B*, *KMT2F/KMT2G* and *KMT2C/D,* and *KMT2E,* an enzymatically inactive protein.[5] Of these Trithorax proteins, only KMT2A and KMT2B can bind to menin, which serves as an adaptor between KMT2A/B and *PSIP1* (PC4 And SRSF1 Interacting Protein 1).[6] Menin-KMT2A inhibitors block the interaction between menin and KMT2A, resulting in displacement of the whole complex from the chromatin. As a consequence, methyltransferase activity of the canonical complex or fusion proteins is lost at these loci, and as a consequence AML development is impaired as shown in several *in vivo* model systems.[7–9] Known target genes of the

KMT2A-complex, including the *HOX* genes and *MEIS1*, are all upregulated in patients with rearranged *KMT2A* and *NPM1* mutations.[10–15]

The importance of the tumor microenvironment (TME) in cancer disease development in general and also specifically in AML has become more and more evident.[16] By inducing alterations in the TME, leukemic blasts benefit in terms of drug resistance driving relapse of disease.[17,18] One of the escape strategies of leukemic blasts is MHC class I and class II loss or decreased expression through genetic deletion or epigenetic downregulation, which renders them invisible to T cells due to defective antigen presentation. Patients that relapse after allogeneic hematopoietic stem cell transplant (allo-HSCT) show significant lower expression of MHC class I and class II molecules, indicating a role of MHC class I and II antigen presentation in the effectivity of allo-HSCT and other immunotherapies.[18–20] It will be of great interest to develop new strategies to reverse the downregulation of MHC class I and II molecules to further improve the efficacy of immunotherapies.

Here, we show that the novel menin-KMT2A inhibitor JNJ-75276617 (bleximenib) impairs proliferation and drives differentiation of primary AML patient cells. We setup a drug screen in which genetic alterations and the quantitative proteome were compared with drug efficacy in a preclinical setting, which revealed that GMP-like AMLs displayed the greatest sensitivity. We find that not only *NPM1c*/*DNMT3A*^{mut} AMLs are sensitive, but that also some *NPM1*^{wt} AML subtypes without *KMT2A*-*MLLT3* rearrangements benefit from menin-KMT2A inhibition upon treatment with JNJ-75276617. Genome-wide ChIPseq studies revealed patient-specific epigenetic alterations upon JNJ-75276617 treatment, revealing a striking upregulation of MHC class I and class II expression as a consequence of epigenetic changes upon menin-

KMT2A inhibition, which functionally resulted in enhanced sensitivity of leukemic blasts to T cell-mediated cytotoxicity.

Methods

Primary samples

AML blasts from peripheral blood or bone marrow from untreated patients were studied after informed consent and the protocol was approved by the Medical Ethical Committee of the University Medical Center Groningen, The Netherlands, in accordance with the Declaration of Helsinki. Mononuclear cells (MNCs) were isolated via Lymphoprep^{TM} separation and cryopreserved. Next Generation Sequencing was performed to obtain mutation status of primary AML cells using the TruSight Myeloid Sequencing Panel (Illumina) or exome sequencing. Neonatal cord blood (CB) samples were obtained from healthy full-term pregnancies at the obstetrics departments at the Martini Hospital and University Medical Center Groningen.

Menin-KMT2A inhibitor screen in primary AML samples

Cryopreserved mononuclear cells (MNCs) of AML patients (Supplemental Table 1) were thawed, resuspended in newborn calf serum (NCS) supplemented with DNase I (20 U/mL), 4 µM $MgSO_4$ and heparin (5 U/mL) and incubated for 15 min at 37°C. MNCs were either cultured in liquid culture supplemented with G-CSF (Amgen), N-Plate (TPO)(Amgen) and IL-3 (Sandoz) (all 20 ng/mL) or co-cultured in Gartner's medium supplemented with cytokines on MS5, which were confluent plated on 0.1% gelatin-coated 48 wells plates and pre-treated with Mitomycin C. MNCs were treated with DMSO or 0.03, 0.30 and 3.00 µM JNJ-75276617 inhibitor for 14 days. Fresh medium and inhibitor were added at day 7 after demi-population of the cells. On day

7 and 14 cells were stained with CD45-PECy7 (BioLegend; 304016), CD117-PE (ImmunoTools; 21271174X2), CD11b-FITC (ImmunoTools; 21279113X2), and DAPI (ThermoScientific) in a 96 wells plate, and were incubated for 30 min at 4°C. Fluorescence measurements were taken using a MACSQuant X Flow Cytometer (Miltenyi Biotec)

Further details can be found in the Supplemental Methods section

Results

Heterogeneity in sensitivity to menin-KMT2A inhibition across the diverse genetic landscape of AML

Recently, clinical trial with menin-KMT2A interaction inhibitors showed a positive response in *KMT2A*-rearranged and *NPM1*-mutated leukemias.[7,21,22] Although other AML subtypes, like NUP98-rearranged leukemias[23] and UBTF-TD leukemia[24], were sensitive to menin-KMT2A interaction inhibitors, little has been revealed about the efficacy across the heterogeneous genetic landscape of AML and the mechanisms of action. JNJ-75276617 is a novel potent and selective inhibitor of the binding between menin and KMT2A.[1] To be able to link menin-KMT2A inhibitor sensitivity to protein expression profiles and genotypes we performed a drug screen in a panel of 37 primary AML blast samples for which we generated a full label-free quantitative proteome (n=22) and performed Illumina TruSight sequencing (n=30) to obtain mutation status. Samples were treated with 0.03-3.0 µM JNJ-75276617 in liquid (LQ) culture or MS5 co-culture for 7 and 14 days, and effects on proliferation, viability and differentiation were monitored by flow cytometry (Supplemental figure 1A-B). Area under the curve (AUC) values were determined based on viable $DAPI^-/CD45^{dim}$ blast

counts, which revealed strong efficacy but also heterogeneity in responses divided in high, late, early and low sensitivity towards JNJ-75276617 (Figure 1A, Supplemental figure 1C, Supplemental figure 2). We also screened a panel of AML cell lines and our primary cord blood (CB)-derived *KMT2A-AF9* AML model[15] which again revealed heterogeneity in responses, whereby the *KMT2A*-rearranged and *NPM1c* AMLs were most sensitive (Figure 1B-C). Although slight differences in sensitivity were observed between liquid cultures and MS5 cocultures for some AMLs, these did not reach significance and in general we observed that when AMLs were sensitive, this was true under both liquid culture as well as MS5 bone marrow stromal coculture growth conditions (Supplemental figure 3C-D). Normal healthy $CD34^+$ cells were considerably less sensitive compared to AMLs, both under liquid culture and MS5 stromal coculture conditions, with AUC values well above 2.5 (Figure 1D). We considered samples below 2.5 to be sensitive. To gain more insight in the genetic component in the differential sensitivity to menin-KMT2A inhibition, we compared AUC values with mutational status. *NPM1c/DNMT3A*^{mut} was the strongest predictor for sensitivity, particularly at day 14 (Figure 1E, Supplemental figure 3A). Interestingly however, we also identified strong efficacy in several *NPM1*^{wt} GMP-like AML samples without *KMT2A-MLLT3* rearrangements (Figure 1A, AML22, AML11, AML15, AML4 and AML45). AML22 did have a *KMT2A-EP300* rearrangement, in line with the notion that *KMT2A*-rearranged AML is sensitive to menin-KMT2A-inhibition.[7,25,26] AML4 had a *CEBPA* mutation and AML15 had a *NUP98*-rearrangement and a *CEBPA* mutation, which both have also been shown to be sensitive in cell lines towards menin-KMT2A inhibition by VTP50469 (*NUP98*) or MI-463 and MI-503 (*CEBPA*).[23,27] Four other AMLs with a *CEBPA* mutation (AML61, AML17, AML62 and AML3) were slower responders and showed a decrease in proliferation at LQ day 14. AML11 and AML45

both had a RUNX1 mutation, which has also been shown to be sensitive towards menin-KMT2A inhibition in one case in the clinical trial Ziftomenib (KO-539).[28] Less sensitive RUNX1 and/or *CEBPA* mutated AMLs in our cohort often coincided with *TET2* mutations and in AML60 with a *RAS* mutation. To further investigate efficacy of JNJ-75276617 in AML patient samples with fusion-protein aberrations, we additionally treated four *KMT2A-MLLT3*, one *NUP98-r* and two *NPM1-MLF* primary AML samples (Supplemental Figure 3B, also added to Figure 1A). After 7 days of treatment 2/7 LQ cultured samples and 4/7 MS5 co-cultured samples were sensitive to the inhibitor. Although no effect was observed on proliferation after 7-day-treatment of menin-KMT2A in AML35 and AML33, an effect on differentiation measured by CD11b expression was found. AML37 and AML38 not only showed reduced proliferation after menin-KMT2A treatment, but also displayed a strong induction of CD11b expression. This would suggest that a combination read-out of proliferation (AUC values) and differentiation induction would be advisable. Therefore, the effects of menin-KMT2A inhibition on differentiation were investigated in further detail. CD11b was significantly increased upon menin-KMT2A inhibition, which was observed for AMLs where proliferation was also strongly inhibited (Figure 2A, Supplemental figure 4A, black curves), but also in cases where proliferation was less affected by menin-KMT2A inhibition (Figure 2A, Supplemental figure 4A, red curves). To address this further, AUC (proliferation) values and change in CD11b expression were compared, revealing AML samples that responded in terms of inhibition of proliferation, induction of differentiation, or both (Figure 2B, Supplemental figure 4B). To gain more insight into these phenomena, the $CD45^{dim}$ blast population was distinguished from the more myeloid committed/monocytic $CD45^{high}/SSC^{high}$ population by flow cytometry (Figure 2D), and effects on

proliferation versus differentiation were analyzed which again revealed heterogeneous responses. For example, in the more immature AML17 JNJ-75276617 treatment resulted in a clear block in proliferation of the $CD45^{dim}$ blast population while a strong increase in more myeloid committed/monocytic $CD45^{high}/SSC^{high}$ differentiated cells was observed (Figure 2C), coinciding with a strong increase in CD11b (Figure 2E). AML13 was a more committed AML subtype with a larger proportion of $CD45^{high}/SSC^{high}$ cells at diagnosis. Here, total cell counts of both the blast-like cells as well as the more committed monocyte-like cells were reduced (Figure 2C), again coinciding with an increase in CD11b (Figure 2C-E). A strong induction in CD11b expression was also noted in our CB *KMT2A-AF9* model[15] (Supplemental figure 4C), coinciding with clear morphological myeloid differentiation (Supplemental figure 4D). The induction of differentiation was most pronounced in *NPM1c* and $DNMT3A^{mut}$ cases (Supplemental figure 4E).

Quantitative proteome analyses links menin-KMT2A inhibitor sensitivity to more committed L-GMP-type AMLs

To obtain a better understanding of the protein expression programs that underlie menin-KMT2A inhibitor sensitivity we analyzed the full proteome of a set of 22 primary AML samples. We calculated Pearson correlations between the quantitative proteome dataset and AUC values of LQ day 7 (Supplemental figure 5A) or MS5 day 7 (Supplemental figure 5D). Ranked Pearson correlation lists were then used for gene set enrichment analysis (GSEA), which revealed that menin-KMT2A inhibitor-sensitive AMLs were enriched for signatures related to L-GMPs, neutrophil degranulation, *KMT2A*-rearranged leukemias and *NPM1c*-mutated leukemias, which was seen in both liquid cultures as well as MS5 cocultures (Supplemental figure 5B-

C, Figure 3A, Supplemental figure 5E). These data suggest that somewhat more committed, L-GMP-type AMLs are most sensitive to menin-KMT2A inhibition. To further analyse these findings, we performed single sample GSEA (ssGSEA) on the full proteome to identify the maturation status of the AML samples (Figure 3B) and subsequently compared AUC values between GMP-like, mixed and HSC-like AMLs, which showed a significant higher sensitivity to JNJ-75276617 in GMP-like AML cultured on MS5 (Figure 3C) and a trend towards sensitivity in LQ cultured samples (Supplemental figure 6D). Since we identified that AML patient samples with *NPM1c* and *DNMT3A* mutations showed an increased sensitivity towards menin-KMT2A inhibition, we wondered whether *NPM1c* and *DNMT3A*^{wt} samples were more HSC-like and double mutant AML samples more GMP-like. While *NPM1c* mutations were present in all three populations, *NPM1*c/*DNMT3A*^{wt} AMLs were exclusively found in HSC-like and Mixed populations (Figure 3B). In addition, GMP-like *NPM1c* AMLs were always *DNMT3A*^{mut} *as well.* To further substantiate these findings in larger patient cohorts we performed GSEA analysis in the TCGA and our own quantitate proteome dataset comparing *NPM1*c/*DNMT3A*^{mut} AMLs with *NPM1*c/*DNMT3A*^{wt} AMLs identified that *NPM1*c/*DNMT3A*^{mut} AMLs were indeed significantly more GMP-like (Supplemental figure 6E-F). Reversely, we observed that lower sensitivity was associated with more immature phenotypes linked to GSEA terms such as “HSC UP”, “poor prognosis AML genes”, “RRNA processing” and “chromatin modifying enzymes” (Supplemental figure 5B-C, Figure 3B, Supplemental figure 5D). These analyses were repeated by only focussing on *NPM1*^{wt} AML samples, and also within this genetic subgroup we observed that more committed L-GMP-type AMLs were the most sensitive while immature LSC-type AMLs were less sensitive to menin-KMT2A inhibition (Supplemental figure 6C). MEIS1, HOXA proteins and IGF2BP2 are

frequently upregulated in *NPM1*c AML (Supplemental figure 5F), and *MEIS1* and *IGF2BP2* are also downregulated upon menin-KMT2A inhibition (Figure 4B, Supplemental figure 7). However, we did not observe correlations between JNJ-75276617 inhibitor sensitivity and MEIS1, HOXA10 or IGF2BP2 baseline expression (Supplemental figure 6A-B).

ChIPseq reveals common and AML-specific targets upon menin-KMT2A inhibition

To further evaluate the targets of menin-KMT2A we performed chromatin immunoprecipitation (ChIP) sequencing in 3 primary AML patient samples (AML2, *NPM1c*/*DNMTA*^{mut}/*FLT3*-ITD/*RUNX1*^{mut}; AML5, *NPM1c*/*DNMTA*^{mut}/*FLT3*-ITD and AML22, *TET2*^{mut}/*SRSF2*^{mut}/*KMT2A-EP300*) and the OCI-AML3 cell line (*NPM1c)* after a four-day treatment with DMSO or JNJ-75276617 inhibitor. We first analyzed genome-wide changes after menin-KMT2A inhibition and noticed that H3K4me3 marks were slightly reduced in AML2, while they were slightly increased in the other samples (Figure 4A). H3K27ac marks were overall increased in 3 out of 4 cases, but reduced in AML5. We then analyzed specific loci, and observed a consistent loss of H3K27ac marks at the *MEIS1* locus in all samples, coinciding with a loss of H3K4me3 marks (Figure 4B). At the *HOXA* locus we observed that epigenetic changes were less prominent. We noted that the active H3K4me3/H3K27ac state of the *MEIS1* locus was reverted to a Polycomb repressed state characterized by an increase in H3K27me3 upon menin-KMT2A inhibition (Figure 4B).

When comparing common and AML-specific targets it was clear that MEIS1 plays a very central role upon menin-KMT2A inhibition, and also other previously described targets like FLT3, PBX3, TCF4 and SATB1 displayed reduced H3K4me3 levels in the

majority of cases (Figure 4C). Furthermore, the known menin-KMT2A target *IGF2BP2,* which was recently identified as therapeutic target in AML, was found in our data set as well (Figure 4B-C).[24,29,30,31] Loss of H3K27ac and H3K4me3 at *MEIS1* and *IGF2BP2* loci correlated with significant reductions in mRNA expression, albeit with some heterogeneity, as determined by Q-RT-PCR in proliferation-sensitive (e.g. AML22), differentiation-sensitive (e.g. AML35) or proliferation and differentiation-sensitive AML samples ((e.g. AML5) Supplemental figure 7A). *HOXA9* mRNA expression was less consistently affected across all AML samples upon menin-KMT2A inhibition, with significant downregulation in five samples but significant upregulation in two samples, which appeared to be independent of the effect of the inhibitor on proliferation or differentiation (Supplemental figure 7A). Given the fact that *MEIS1* is transcriptionally repressed after menin-KMT2A inhibition, we wondered whether re-expression of MEIS1 would rescue the observed impaired proliferation, as described previously. Indeed, both OCI-AML3 and MOLM13 cells displayed significantly increased cell counts in the presence of JNJ-75276617 upon MEIS1 overexpression compared to DMSO treated cells (Supplemental figure 7B-C). We also investigated whether re-expression of IGF2BP2 would rescue sensitivity to menin-KMT2A inhibition, and while a slight recue in proliferation was observed, this was not as strong as compared to MEIS1 rescue experiments, indicating that IGF2BP2-independent pathways downstream of MEIS1 must exist as well (Supplemental figure 7D-E). Inhibition of *MEIS1* expression upon treatment with JNJ-75276617 is not prevented by IGF2BP2 overexpression, while *BMI1*, which is a target gene of IGF2BP2, is restored upon IGF2BP2 overexpression (Supplemental figure 7F).

Besides these more common targets, it was interesting to note that a lot of the epigenetic changes induced upon menin-KMT2A inhibition were relatively patient-specific. Already at baseline prior to menin-KMT2A inhibition, the epigenetic landscapes differed considerably between patients, in line with what we and others observed previously,[32,33] potentially also as a consequence of differences in maturation stage[41], and we therefore hypothesize that also the epigenetic changes induced upon menin-KMT2A inhibition are different per patient (Figure 4C, Supplemental figure 7A). Despite these patient-specific features, Gene Ontology (GO) analyses on loci at which H3K4me3 or H3K27ac were gained were significantly enriched for processes associated with differentiation, lineage specification and myeloid commitment (Supplemental figure 8C-D, Supplemental figure 9A). Loci at which H3K4me3 marks were lost were significantly enriched for processes associated with cell cycle, apoptosis and response to growth factors (Supplemental figure 8C). GSEA analyses revealed that HSC/LSC and *NPM1c* signatures were generally lost (Supplemental figure 8A, Supplemental Table 2), while differentiation signatures were gained, which also included terms associated with MHC binding, antigen processing and presentation, phagocytosis and IFNγ responses. (Supplemental figure 8B, Supplemental Table 2). Similar changes were observed in OCI-AML3 cells (Supplemental figure 9B).

Menin-KMT2A inhibition drives HLA expression in a MEIS1-independent but CIITA-dependent manner in the case of MHC-II

Since we observed an increase in H3K4me3 marks on loci related to immunity and MHC proteins (Supplemental figure 8B, D, Supplemental figure 9B), we wished to explore this further. We focused on MHC class I (*HLA-A*) and MHC class II (*HLA-*

DPA1/B1 and *HLA-DRA*) loci, and observed an increase in H3K4me3 and H3K27ac levels upon menin-KMT2A inhibition (Figure 5A). This resulted in increased mRNA expression of *HLA-A* and *HLA-DR* in a larger panel of AMLs undergoing a four-day menin-KMT2A inhibitor treatment (Figure 5B), as well as at the protein level determined by flow cytometry (Figure 5C), although there was clear variation between individual AML patient samples as well. HLA-DR was upregulated in the majority of cases, HLA-A was upregulated in 9/25 cases, and in 5/25 cases a consistent significant upregulation of both MHC class I and MHC class II was noted (Supplemental figure 10A-B). In addition, the mRNA expression of *CIITA*, the known transcription factor of MHC class II genes, was significantly upregulated after menin-KMT2A inhibition. When correlating the fold change of *CIITA* and *HLA-DR* between JNJ-75276617 inhibitor versus DMSO treated cells, we identified a strong positive correlation (R^2=0.748)(Supplemental figure 10C). Since *MEIS1* was significantly reduced in JNJ-75276617 inhibitor-treated cells (Supplemental figure 7), we considered whether *MEIS1* could be a negative regulator of *HLA-DR* and other MHC class II genes as described by Eagle *et al.*[34] However, when we compared the fold change in *MEIS1* expression versus *HLA-DR* expression no correlation was observed (Supplemental figure 10D) and HLA-DR was still upregulated upon JNJ-75276617 inhibitor treatment in MEIS1 overexpression models as determined by flow cytometry (Supplemental figure 10E). These data argue that menin-KMT2A controls MHC class II expression in a MEIS1-independent manner. Therefore, we performed ChIP-qPCR and confirmed binding of menin at the *CIITA* and *HLA-DR* loci (Figure 5D). Subsequently, we generated hetero- and homozygous *CIITA* knockout MV4-11 cells (*CIITA*$^{+/-}$ and *CIITA*$^{-/-}$, respectively), which we treated with 0.03, 0.30 or 3.00 µM JNJ-75276617 inhibitor for four days. At baseline, HLA-DR expression was

significantly lower in *CIITA*$^{+/-}$ and *CIITA*$^{-/-}$ cells in comparison to MV4-11 scrambled (SCR) cells (Figure 5E-G). Upon JNJ-75276617 treatment, HLA-DR expression was dose-dependently upregulated in MV4-11 SCR, but not in *CIITA*$^{-/-}$ cells. These data indicate that the menin-KMT2A complex directly regulates *HLA-DR* loci in a CIITA-dependent manner.

Menin-KMT2A inhibition enhances T cell cytotoxicity

Next, we functionally evaluated whether JNJ-75276617 inhibitor treatment would increase their sensitivity to immune cells. First, the AML cell lines MOLM13 and MV4-11 were pre-treated for four days with DMSO or 0.3 µM and 0.1 µM JNJ-75276617 inhibitor, after which PBMCs were added at different Effector:Target (E:T) ratios for an additional 72 hours. As observed before, menin-KMT2A inhibition resulted in an increase in HLA-DR expression (Figure 6A). Furthermore, menin-KMT2A inhibition impaired cell proliferation as noted before (Figure 6B, 0:1 ratio), but upon the addition of PBMCs a significant further decline in viable cell counts was observed in both cell lines (Figure 6B). Next, we functionally studied T cell cytotoxicity in an allogeneic setting. Primary AML samples (n=8) with different mutational backgrounds were pretreated with 0.3 µM JNJ-75276617 inhibitor for four days, after which cells were washed and antiCD3/CD28 activated T cells from healthy donors were added at different E:T ratios for an additional three days. Four out of eight AML patient samples were found to have an increased sensitivity to allogeneic T cells after menin-KMT2A inhibition (Figure 6C, Supplemental figure 11A). Interestingly, unlike the other four less sensitive primary AML samples, all four sensitive AML samples carried *NPM1c* and *DNMT3A* mutations (Figure 6D). T cell counts were also diminished after co-culture with menin-KMT2A-inhibitor pretreated AMLs that showed increased T cell

cytotoxicity, suggestive for activation-induced cell death after target cell recognition (Supplemental figure 11B).[35] Finally, we evaluated T cell cytotoxicity in an autologous setting. $CD45^+$ blast populations and $CD3^+$ T cell populations were sorted from primary *NPM1c* AML patient samples (n=9, Supplemental table 1). Then, AML blasts were cultured in either the absence (depleted) or presence (enriched) of their own T cells at a fixed ratio, in the absence or presence 0.3 µM JNJ-75276617 inhibitor. Like we observed before, menin-KMT2A inhibition resulted in cell intrinsic cytotoxicity in the absence of T cells, but upon menin-KMT2A inhibition a further significant enhanced T cell cytotoxicity was observed (Figure 7A-C), coinciding with increased MHC class I and MHC class II expression (Figure 7D-E). The strength of the T cell cytotoxic response was not directly correlated to the level of MHC upregulation, indicating that also other mechanisms such as potential tumor cell intrinsic immune evasion mechanisms might play a role that shall need to be investigated further. In AML 54 JNJ-75276617 treatment did not result in increased HLA-A upregulation but did induce strong upregulation of HLA-DR. Yet, T cell cytotoxicity was not further enhanced and AML cells even expanded slightly in the presence of allogeneic T cells (Figure 7B-C), which might be related to the observation that intrinsic cell viability was already strongly affected by menin-KMT2A inhibition or that AML cells might respond to the secretion of cytokines like IFNγ upon T cell activation. However, additional studies are required to obtain further insight into the exact underlying mechanisms. No change CD4/CD8 ratio or CD69 expression was noted upon JNJ-75276617 treatment (Supplemental figure 11C-D). Together, these data indicate that menin-KMT2A inhibition not only impairs long-term self-renewal and drive differentiation of leukemic blasts via cell intrinsic mechanisms, but may also decrease their immune evasion capacity.

Discussion

Inhibitors that target the menin-KMT2A interaction have appeared as a potential new therapeutic approach for patients harbouring *KMT2A*-rearrangements or *NPM1c* mutations. Various in-human trials have now been initiated, but much is still unknown about the exact cell biological processes and downstream molecular mechanisms that mediate inhibitor-induced phenotypes across the heterogeneous AML landscape. Here, we describe that the novel menin-KMT2A inhibitor JNJ-75276617 impairs proliferation and drives differentiation of primary AML patient samples, whereby GMP-like AMLs displayed the greatest sensitivity. Inhibitor sensitivity is not restricted to *NPM1c/DNMT3A*^{mut} and *KMT2A*-rearranged AMLs, but also *NPM1*^{wt} AML subtypes that do carry *CEBPA* mutations or *NUP98*-rearrangements were sensitive to JNJ-75276617. Furthermore, inhibitor sensitivity should not only be determined by reduction in proliferation, but a combination read-out with induction of differentiation and proliferation would be advisable. Mechanistically, we uncover that T cell-mediated cytotoxicity is enhanced in leukemic blasts as a consequence of MHC class I and MHC class II upregulation.

Several menin-KMT2A inhibitors are currently being tested in clinical trials to evaluate safety/efficacy in relapsed or refractory AML with *NPM1c* or *KMT2A* rearrangements, including KO-539, SNDX-5613, DS-1594b and JNJ-75276617.[36–38] In the phase I trial of SNDX-5613 (revumenib) 68 patients were enrolled and treated. 46 patients had *KMT2A*-rearrangements, 14 had *NPM1c* and eight patients lacked both mutations.[22] Within these 68 patients there were no responses found in the eight patients without *KMT2A*-rearrangements or *NPM1* mutations. Two patients had a *NPM1* and *DNMT3A* mutation of which one responded to revumenib. In the KO-539 trial one

patient harbouring *NPM1*, *DNMT3A* and *KMT2D* mutations treated at 200 mg/day achieved a MRD-negative complete remission for >100 weeks.[28] Interestingly, in this trial also response rates were reported in patients that did not carry *NPM1* or *KMT2A*-r mutations. Our data would argue that a particular interest should go to patients that carry both *NPM1c* and *DNMT3A* mutations or *KMT2A*-rearrangements, but that also a subset of *NPM1*^{wt}/*KMT2A*^{wt} patients might benefit, particularly in the context of *CEBPA* and *RUNX1* mutations or *NUP98*-rearrangements.

Our data indicates that a common signature that is affected in all tested cases upon menin-KMT2A inhibition entails known targets *MEIS1* and *IGF2BP2*. Expression of these genes is strongly downregulated upon JNJ-75276617 treatment, resulting in loss of long-term proliferation of leukemic blasts, coinciding with an induction of differentiation. MEIS1 has been identified as an important transcription factor that controls self-renewal of HSCs and LSCs.[14,39–41] One of its targets is IGF2BP2, which was recently shown to control the transcriptional state and maintenance of hematopoietic stem cells[42] and was identified as a potential therapeutic target in AML.[43] Mechanistically, IGF2BP2 acts as an m^{6}A reader, thereby regulating mRNA abundance in HSCs, and deficiency of IGF2BP2 resulted in loss of HSC function.[42] We observed that *MEIS1* expression is directly correlated with *IGF2BP2* expression levels, and while re-expression of exogenous MEIS1 was able to partially rescue cell proliferation of JNJ-75276617-treated cells, in line with previous data,[21,23] we only observed a minor rescue in proliferation and target gene expression upon IGF2BP2 overexpression. These data clearly indicate that multiple pathways downstream of menin are relevant in conveying phenotypes, which cannot exclusively be explained by *IGF2BP2* changes.

Besides loss of H3K4me3 marks on targets such as *MEIS1* and *IGF2BP2* upon inhibition of the interaction between menin and KMT2A, we also find that various loci become activated, as shown by an increase in H3K27ac and H3K4me3. There was considerable heterogeneity in upregulated targets between individual AML patients upon menin-KMT2A inhibition. At baseline prior to menin-KMT2A inhibition, the epigenetic landscapes already differed considerably between patients, in line with what we and others observed previously,[32,33] potentially also as a consequence of differences in maturation stage[41] and we therefore hypothesize that also the epigenetic changes induced upon menin-KMT2A inhibition are rather AML patient-specific. But what was common in all cases is that genes associated with myeloid differentiation programs and immune functions become activated, in line with what we observed phenotypically. While further studies are needed to obtain mechanistic insights driving gene activation, a possibility could be that loci with increased H3K4me3 expression undergo a switch from occupancy by menin-KMT2A to SETD1A and SETD1B with KMT2A as was shown by Sparbier *et al.* for MHC class I expression.[44] Extensive further analyses, including the development of CRISPR KO models, would be required to causally link SETD1A and/or SETD1B to *CIITA* expression control. In addition, it was recently elegantly shown using CRISPR screens in murine *KMT2A-AF9* leukemia models that durable menin-KMT2A inhibition-induced phenotypes depend on KMT2C/D-UTX.[45] Upon inhibition, the menin-KMT2A complex was replaced by the KMT2C/D-UTX complex which was necessary to maintain expression specifically of differentiation genes. However, KMT2A-AF9-driven MEIS1 expression did not depend on UTX. It will be interesting to determine whether the menin-KMT2A to KMT2C/D-UTX switch also drives differentiation programs in human AML patient samples, and also whether potential

resistance to menin-KMT2A inhibitors would be linked to a failure to install this switch. In the same study, it was noted that all members of the non-canonical PRC1.1 complex are required to maintain long-term sensitivity to menin-KMT2A inhibition, since loss of PCGF1, BCOR or KDM2B rendered murine *KMT2A-AF9* cells resistant.[45] It is tempting to speculate that loci that become downregulated upon menin-KMT2A inhibition, such as the *MEIS1* locus, depend on Polycomb group proteins to maintain long-term repression, and we indeed observed an increase in H3K27me3 marks at the *MEIS1* locus, which we aim to further investigate in future studies.

Finally, we reveal that treatment with the JNJ-75276617 inhibitor results in upregulation of HLA-A and HLA-DR in our primary AML cohort and cell lines. While a previous report suggested that MEIS1 would be a negative regulator of HLA-DR expression,[34] we were unable to validate this regulatory mechanism in our setting as there appeared to be no correlation with loss of MEIS1 expression and upregulation of HLA-DR. Rather, we observe strong correlations between HLA-DR and expression of its transcriptional regulator CIITA, and we therefore propose that the induction of MHC-II molecules is MEIS1 independent. In line, re-expression of MEIS1 failed to impair JNJ-75276617-induced upregulation of HLA-DR, and we also observe direct binding of menin to both the *CIITA* and *HLA-DR* loci. Functionally, we observe that the upregulation of MHC class I and MHC class II molecules results in enhanced cytotoxicity, both in allogeneic and autologous T cell cytotoxicity assays. Sparbier *et al.* also report that treatment with a menin-KMT2A inhibitor resulted in upregulation of MHC molecules.[44] In K562 cells in which MHC class I genes are in a bivalent state characterized by both H3K4me3 and H3K27me3 marks, it was shown that both Polycomb group proteins as well as expression of the menin-KMT2A complex is

required to maintain repression of the locus. Functionally, it was shown that pre-treatment of cells with the menin-KMT2A inhibitor VTP-50469 before co-culture with OT-I T cells enhanced MHC class I-mediated tumor cell killing significantly, thereby providing a direct link between MHC class I upregulation, antigen presentation and increased immunogenicity upon inhibition of menin-KMT2A.[44] After initial chemotherapy treatment a majority of the patients receive an allogeneic hematopoietic stem cell transplant (allo-HSCT) but unfortunately ~20% of the patients still relapse within 5 years.[46] It was found that these relapsed patients have a significant lower expression of MHC class I and II molecules after allo-HSCT.[18] Patients harboring a *NPM1c* mutation have a relatively favorable prognosis in the absence of *FLT3*-ITD mutations and in *NPM1c* mutated patients without *FLT3*-ITD mutations allo-HSCT in first-line treatment seems to be beneficial for survival.[47,48] This might be because mutated NPM1 is localized to the cytoplasm, where it can be processed by the MHC class I or II degradation pathway leading to the presentation of NPM1 mutant peptides by HLA molecules[49] initiating a leukemia-specific autologous T-cell cytotoxicity against these *NPM1c* peptides.[36,50] Obviously, the efficacy of cytotoxicity heavily depends on appropriate expression of MHC class I and MHC class II molecules, and our data indicate that menin-KMT2A inhibition can potentially add therapeutic benefit by reactivating antigen presentation machinery.

References

1. Kwon MC, Thuring JW, Querolle O, et al. Preclinical efficacy of the potent, selective menin-KMT2A inhibitor JNJ-75276617 (bleximenib) in KMT2A- and NPM1-altered leukemias. Blood. 2024;144(11):1206-1220.

2. Miller CA, Wilson RK, Ley TJ. Genomic landscapes and clonality of de novo AML. N Engl J Med. 2013;369(15):1473.

3. de Boer B, Prick J, Pruis MG, et al. Prospective Isolation and Characterization of Genetically and Functionally Distinct AML Subclones. Cancer Cell. 2018;34(4):674-689.e8.

4. Klco JM, Spencer DH, Miller CA, et al. Functional heterogeneity of genetically defined subclones in acute myeloid leukemia. Cancer Cell. 2014;25(3):379-392.

5. Yang W, Ernst P. SET/MLL family proteins in hematopoiesis and leukemia. Int J Hematol. 2017;105(1):7-16.

6. Yokoyama A, Cleary ML. Menin critically links MLL proteins with LEDGF on cancer-associated target genes. Cancer Cell. 2008;14(1):36-46.

7. Krivtsov A V, Evans K, Gadrey JY, et al. A Menin-MLL Inhibitor Induces Specific Chromatin Changes and Eradicates Disease in Models of MLL-Rearranged Leukemia. Cancer Cell. 2019;36(6):660-673.e11.

8. Borkin D, He S, Miao H, et al. Pharmacologic inhibition of the Menin-MLL interaction blocks progression of MLL leukemia in vivo. Cancer Cell. 2015;27(4):589-602.

9. Chen Y-X, Yan J, Keeshan K, et al. The tumor suppressor menin regulates hematopoiesis and myeloid transformation by influencing Hox gene expression. Proc Natl Acad Sci U S A. 2006;103(4):1018-1023.

10. Issa GC, Ravandi F, DiNardo CD, Jabbour E, Kantarjian HM, Andreeff M. Therapeutic implications of menin inhibition in acute leukemias. Leukemia. 2021;35(9):2482-2495.

11. Slany RK. The molecular biology of mixed lineage leukemia. Haematologica. 2009;94(7):984-93.

12. Kumar AR, Li Q, Hudson WA, et al. A role for MEIS1 in MLL-fusion gene leukemia. Blood. 2009;113(8):1756-1758.

13. Faber J, Krivtsov A V, Stubbs MC, et al. HOXA9 is required for survival in human MLL-rearranged acute leukemias. Blood. 2009;113(11):2375-2385.

14. Woolthuis CM, Han L, Verkaik-Schakel RN, et al. Downregulation of MEIS1 impairs long-term expansion of CD34+ NPM1-mutated acute myeloid leukemia cells. Leukemia. 2012;26(4):848-853.

15. Horton SJ, Jaques J, Woolthuis C, et al. MLL-AF9-mediated immortalization of human hematopoietic cells along different lineages changes during ontogeny. Leukemia. 2013;27(5):1116-1126.

16. Weinhäuser I, Pereira-Martins DA, Almeida LY, et al. M2 macrophages drive leukemic transformation by imposing resistance to phagocytosis and improving mitochondrial metabolism. Sci Adv. 2023;9(15):eadf8522.

17. Vadakekolathu J, Minden MD, Hood T, et al. Immune landscapes predict chemotherapy resistance and immunotherapy response in acute myeloid leukemia. Sci Transl Med. 2020;12(546):eaaz0463.

18. Toffalori C, Zito L, Gambacorta V, et al. Immune signature drives leukemia escape and relapse after hematopoietic cell transplantation. Nat Med. 2019;25(4):603-611.

19. Christopher MJ, Petti AA, Rettig MP, et al. Immune Escape of Relapsed AML Cells after Allogeneic Transplantation. N Engl J Med. 2018;379(24):2330-2341.

20. Jan M, Leventhal MJ, Morgan EA, et al. Recurrent genetic HLA loss in AML relapsed after matched unrelated allogeneic hematopoietic cell transplantation. Blood Adv. 2019;3(14):2199-2204.

21. Uckelmann HJ, Kim SM, Wong EM, et al. Therapeutic targeting of preleukemia cells in a mouse model of NPM1 mutant acute myeloid leukemia. Science. 2020;367(6477):586-590.

22. Issa GC, Aldoss I, DiPersio J, et al. The menin inhibitor revumenib in KMT2A-rearranged or NPM1-mutant leukaemia. Nature. 2023;615(7954):920-924.

23. Heikamp EB, Henrich JA, Perner F, et al. The menin-MLL1 interaction is a molecular dependency in NUP98-rearranged AML. Blood. 2022;139(6):894-906.

24. Barajas JM, Rasouli M, Umeda M, et al. Acute myeloid leukemias with UBTF tandem duplications are sensitive to menin inhibitors. Blood. 2024;143(7):619-630.

25. Dafflon C, Craig VJ, Méreau H, et al. Complementary activities of DOT1L and Menin inhibitors in MLL-rearranged leukemia. Leukemia. 2017;31(6):1269-1277.

26. Yokoyama A, Somervaille TCP, Smith KS, Rozenblatt-Rosen O, Meyerson M, Cleary ML. The menin tumor suppressor protein is an essential oncogenic cofactor for MLL-associated leukemogenesis. Cell. 2005;123(2):207-218.

27. Schmidt L, Heyes E, Scheiblecker L, et al. CEBPA-mutated leukemia is sensitive to genetic and pharmacological targeting of the MLL1 complex. Leukemia. 2019;33(7):1608-1619.

28. Erba HP, Fathi AT, Issa GC, et al. Update on a Phase 1/2 First-in-Human Study of the Menin-KMT2A (MLL) Inhibitor Ziftomenib (KO-539) in Patients with Relapsed or Refractory Acute Myeloid Leukemia. Blood. 2022;140(Supplement 1):153-156.

29. Olsen SN, Godfrey L, Healy JP, et al. MLL::AF9 degradation induces rapid changes in transcriptional elongation and subsequent loss of an active chromatin landscape. Mol Cell. 2022;82(6):1140-1155.e11.

30. Uckelmann HJ, Haarer EL, Takeda R, et al. Mutant NPM1 Directly Regulates Oncogenic Transcription in Acute Myeloid Leukemia. Cancer Discov. 2023;13(3):746-765.

31. Weng H, Huang F, Yu Z, et al. The m6A reader IGF2BP2 regulates glutamine metabolism and represents a therapeutic target in acute myeloid leukemia. Cancer Cell. 2022;40(12):1566-1582.e10.

32. Yi G, Wierenga ATJ, Petraglia F, et al. Chromatin-Based Classification of Genetically Heterogeneous AMLs into Two Distinct Subtypes with Diverse Stemness Phenotypes. Cell Rep. 2019;26(4):1059-1069.e6.

33. van den Boom V, Maat H, Geugien M, et al. Non-canonical PRC1.1 Targets Active Genes Independent of H3K27me3 and Is Essential for Leukemogenesis. Cell Rep. 2016;14(2):332-346.

34. Eagle K, Harada T, Kalfon J, et al. Transcriptional Plasticity Drives Leukemia Immune Escape. Blood Cancer Discov. 2022;3(5):394-409.

35. Chappell DB, Restifo NP. T cell-tumor cell: a fatal interaction? Cancer Immunol Immunother. 1998;47(2):65-71.

36. Ranieri R, Pianigiani G, Sciabolacci S, et al. Current status and future perspectives in targeted therapy of NPM1-mutated AML. Leukemia. 2022;36(10):2351-2367.

37. Iwama A, Oguro H, Negishi M, et al. Enhanced self-renewal of hematopoietic stem cells mediated by the polycomb gene product Bmi-1. Immunity. 2004;21(6):843-851.

38. Yuan J, Takeuchi M, Negishi M, Oguro H, Ichikawa H, Iwama A. Bmi1 is essential for leukemic reprogramming of myeloid progenitor cells. Leukemia. 2011;25(8):1335-1343.

39. Unnisa Z, Clark JP, Roychoudhury J, et al. Meis1 preserves hematopoietic stem cells in mice by limiting oxidative stress. Blood. 2012;120(25):4973-4981.

40. Kocabas F, Zheng J, Thet S, et al. Meis1 regulates the metabolic phenotype and oxidant defense of hematopoietic stem cells. Blood. 2012;120(25):4963-4972.

41. Kumar AR, Sarver AL, Wu B, Kersey JH. Meis1 maintains stemness signature in MLL-AF9 leukemia. Blood. 2010;115(17):3642-3643.

42. Yin R, Chang J, Li Y, et al. Differential m6A RNA landscapes across hematopoiesis reveal a role for IGF2BP2 in preserving hematopoietic stem cell function. Cell Stem Cell. 2022;29(1):149-159.e7.

43. Cheng Y, Gao Z, Zhang T, et al. Decoding m(6)A RNA methylome identifies PRMT6-regulated lipid transport promoting AML stem cell maintenance. Cell Stem Cell. 2023;30(1):69-85.e7.

44. Sparbier CE, Gillespie A, Gomez J, et al. Targeting Menin disrupts the KMT2A/B and polycomb balance to paradoxically activate bivalent genes. Nat Cell Biol. 2023;25(2):258-272.

45. Soto-Feliciano YM, Sánchez-Rivera FJ, Perner F, et al. A Molecular Switch between Mammalian MLL Complexes Dictates Response to Menin-MLL Inhibition. Cancer Discov. 2023;13(1):146-169.

46. Devillier R, Forcade E, Garnier A, et al. In-depth time-dependent analysis of the benefit of allo-HSCT for elderly patients with CR1 AML: a FILO study. Blood Adv. 2022;6(6):1804-1812.

47. Greiner J, Schneider V, Schmitt M, et al. Immune responses against the mutated region of cytoplasmatic NPM1 might contribute to the favorable clinical outcome of AML patients with NPM1 mutations (NPM1mut). Blood. 2013;122(6):10871088.

48. Aldoss I, Nakamura R, Yang D, et al. Favorable outcomes for allogeneic hematopoietic cell transplantation in elderly patients with NPM1-mutated and FLT3-ITD-negative acute myeloid leukemia. Bone Marrow Transplant. 2020;55(2):473-475.

49. Liso A, Colau D, Benmaamar R, et al. Nucleophosmin leukaemic mutants contain C-terminus peptides that bind HLA class I molecules. Leukemia. 2008;22(2):424-426.

50. van der Lee DI, Reijmers RM, Honders MW, et al. Mutated nucleophosmin 1 as immunotherapy target in acute myeloid leukemia. J Clin Invest. 2019;129(2):774-785.

Figures

Figure legends

Figure 1. Heterogeneity in sensitivity to menin-KMT2A inhibition across the diverse genetic landscape of acute myeloid leukemia

A. Area under the curve (AUC) values at day 7 and day 14 of the JNJ-75276617 inhibitor drug screen in primary AML patient samples with various mutations in liquid culture. AUC values were calculated to show the effect of the inhibitor on proliferation. AMLs are ordered based on high, late, early and low sensitivity. Grey tile with star (*) annotate not determined (ND) samples. Wild type genes are annotated with a grey tile (WT) and mutated genes are annotated with a red tile (Mut). B. AUC values of the JNJ-75276617 inhibitor drug screen in 10 AML cell lines. Wild type genes are annotated with a grey tile (WT) and mutated genes with a purple tile (Mut). C. Dose-dependent effects on cell viability upon treatment of CB KMT2A-AF9 with JNJ-75276617 under liquid culture conditions. D. Paired analysis of AUC values calculated for the effect of JNJ-75276617 inhibitor treatment on LQ and MS5 co-cultured healthy $CD34^+$ cells on day 7 (n=6, biological replicates). E. Boxplots showing AUC values of *DNMT3A*^{mut} versus *DNMT3A*^{WT} in *NPM1c* primary AML patient samples on LQ day 7, 14 and MS5 day 14. Statistical analysis by unpaired Student's t test or paired for panel D. * $P < 0.05$, ** $P < 0.01$, *** $P < 0.001$.

Figure 2. Menin-KMT2A inhibition induces differentiation in leukemic blast cells

A. Lineplots showing the MFI of CD11b normalized to the DMSO control for LQ day 7 (n=19). Black curves represent samples in which JNJ-75276617 also blocked proliferation, red curves represent samples in which proliferation was less effected by

JNJ-75276617 treatment. B. Comparison between AUC and CD11b expression (normalized to DMSO control) identifying 4 groups: proliferation, differentiation and proliferation, differentiation only, and weak responders. Red dots represent samples in which proliferation was less effected by menin-KMT2A inhibition. C. Absolute cell counts for gates B and M showing dose-dependent effect on proliferation of the JNJ-75276617 inhibitor on LQ day 7. D. Flow cytometry plots of AML17 and AML13 on LQ day 7. Depicted are CD45 expression and side scatter (SSC) for DMSO, 0.03, 0.3 and 3.0 µM JNJ-75276617 inhibitor. Gates are drawn for blast-like (B) and monocyte-like (M) cell populations. E. Barplots depicting the MFI of CD11b normalized to the DMSO control for AML17 and on LQ day 7. Statistical analysis by unpaired Student's t test. * $P < 0.05$, ** $P < 0.01$, *** $P < 0.001$.

Figure 3. Quantitative proteome analyses links menin-KMT2A inhibitor sensitivity to more committed L-GMP-type acute myeloid leukemias

A. Dotplot of gene set enrichment analysis (GSEA) signatures enriched in sensitive and less sensitive primary AML samples at MS5 day 7. B. Selection of single sample GSEA (ssGSEA) terms from proteome dataset AML samples to identify maturation state. HSC-like, GMP-like and Mixed samples were identified. DNMT3A and NPM1c was annotated, whereby grey is wildtype (WT) and red is mutated (Mut). C. Comparison between AUC values in GMP-like, mixed and HSC-like groups of MS5 day 7. Statistical analysis by unpaired Student's t test.

Figure 4. ChIPseq reveals common and acute myeloid leukemia-specific targets upon menin-KMT2A inhibition

A. Average plots showing genome wide H3K27ac and H3K4me3 changes after menin-KMT2A inhibition for four days in AML2, AML22, AML5 and OCI-AML3 cells. B. H3K27ac, H3K4me3 and H3K27me3 chromatin immunoprecipitation sequencing (ChIP-seq) tracks of AML2, AML22, AML5 and OCI-AML3 cells treated with DMSO or 0.03 (AML22)/0.3 µM JNJ-75276617 inhibitor for four days showing *MEIS1*, *IGF2BP2* and the *HOXA* cluster. C. VENN diagrams showing overlap in genes with a fold change (FC) < -0.585 for H3K4me3 expression in menin-KMT2A inhibitor JNJ-75276617 versus DMSO treated cells.

Figure 5. Menin-KMT2A inhibition drives HLA expression in a MEIS1-independent but CIITA-dependent manner in the case of MHC class II.

A. H3K27ac and H3K4me3 ChIP-seq tracks of AML2, AML22, AML5 and OCI-AML3 cells treated with DMSO or 0.03 (AML22)/0.3 µM JNJ-75276617 inhibitor for four days showing *HLA-A*, *HLA-DPA1/B1* and *HLA-DRA* loci. B. Barplots showing relative mRNA expression of *HLA-A*, *HLA-DR* and *CIITA* in four-day JNJ-75276617 inhibitor-treated primary AML patient samples normalized to DMSO. Triangles annotate *NPM1c* samples. C. Barplot depicting MFI of HLA-DR in four-day DMSO or JNJ-75276617 inhibitor-treated primary AML patient samples normalized to DMSO. Triangles annotate *NPM1c* samples. D. Barplot showing ChIP-qPCR data of MOLM13 cells with EV-GFP and GFP-Menin using antibodies against GFP. E. Barplot showing MFI of HLA-DR in MV4-11 scrambled (SCR), *CIITA* heterozygous knockout ($CIITA^{+/-}$) and *CIITA* homozygous knockout ($CIITA^{-/-}$) cells treated with

DMSO, 0.03, 0.30 or 3.00 µM JNJ-75276617 inhibitor for four days (n=3). F. MFI of HLA-DR in MV4-11 scrambled, CIITA$^{+/-}$ and CIITA$^{-/-}$ in control cells. G. MFI of HLA-DR in MV4-11 scrambled, CIITA$^{+/-}$ and CIITA$^{-/-}$ cells treated with DMSO, 0.03, 0.30 or 3.00 µM JNJ-75276617 inhibitor for four days. Error bars represent mean ± standard error of the mean (SEM). Statistical analysis by unpaired Student's t test or Simple Linear Regression. * P < 0.05, ** P < 0.01, *** P < 0.001, ns = not significant.

Figure 6. Menin-KMT2A inhibition enhances T cell cytotoxicity

A. Barplots depicting MFI of HLA-DR in DMSO or 0.3 µM JNJ-75276617 inhibitor treated MV4-11 and MOLM13 cells normalized to DMSO. B. Bar- and lineplot showing viable AML counts (barplot) determined by Annexin-V and Zombie NIR™ of different effector:target (E:T) ratio's in DMSO or JNJ-75276617 pre-treated MV4-11 and MOLM13 cells co-cultured with allogeneic T cells for 72 hours. MV4-11 cells were pre-treated with 0.1 µM JNJ-75276617 and MOLM13 cells with 0.3 µM. E:T ratios were normalized to ratio 0:1 (lineplot). C. Lineplots showing normalized viable cell counts, determined by Annexin-V and Zombie NIR™, of different E:T ratio's in 8 primary AML samples, which were pre-treated with DMSO or 0.3 µM JNJ-75276617, co-cultured with allogeneic T cells for 72 hours. E:T ratios were normalized to their DMSO control. D. Tileplot depicting mutational status of primary AML samples used in panel C. Error bars represent mean ± standard error of the mean (SEM). Statistical analysis by unpaired Student's t test. * P < 0.05, ** P < 0.01, *** P < 0.001.

Figure 7. Menin-KMT2A inhibition enhances T cell cytotoxicity

A. Barplot showing relative AML counts in primary AML samples (n=9) treated with DMSO or 0.3 µM JNJ-75276617 inhibitor cultured without T cells (depleted) or with T

cells (enriched). B. Paired comparison of JNJ-75276617 treated primary AML samples cultured without or with T cells. C. Three examples of panel B. D. Paired comparison of MHC class I and MHC class II MFIs of primary AML samples shown in panel B upon 0.3 µM JNJ-75276617 inhibitor treatment. Expression is relative to the DMSO samples. E. MHC class I and MHC class II expression of 3 primary AML samples shown in panel D treated with DMSO or 0.3 µM JNJ-75276617 inhibitor and MHC class II expression of MOLM13 and MV4-11 cells treated with DMSO or 0.3 µM JNJ-75276617 inhibitor. Error bars represent mean ± standard error of the mean (SEM). Statistical analysis by unpaired Student's t test. * $P < 0.05$, ** $P < 0.01$, *** $P < 0.001$.

Figure 1

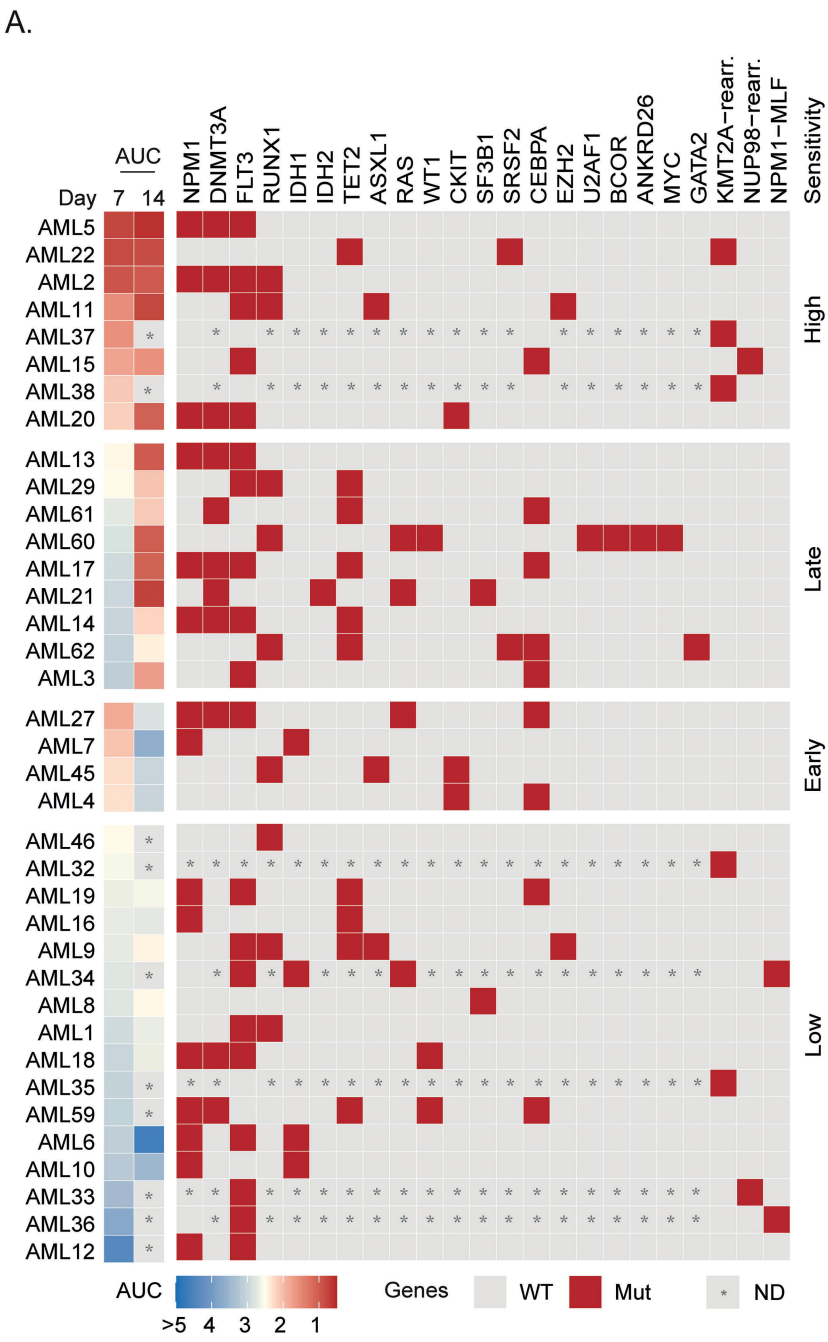
A.
AUC
Day 7 14
NPM1
DNMT3A
FLT3
RUNX1
IDH1
IDH2
TET2
ASXL1
RAS
WT1
CKIT
SF3B1
SRSF2
CEBPA
EZH2
U2AF1
BCOR
ANKRD26
MYC
GATA2
KMT2A−rearr.
NUP98−rearr.
NPM1−MLF
Sensitivity
AML5
AML22
AML2
AML11
AML37
AML15
AML38
AML20
AML13
AML29
AML61
AML60
AML17
AML21
AML14
AML62
AML3
AML27
AML7
AML45
AML4
AML46
AML32
AML19
AML16
AML9
AML34
AML8
AML1
AML18
AML35
AML59
AML6
AML10
AML33
AML36
AML12
High
Late
Early
Low
AUC
>5 4 3 2 1
Genes
WT
Mut
ND

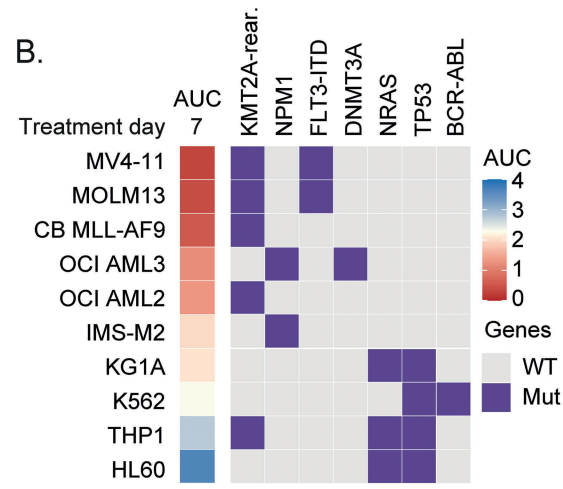
B.
AUC
Treatment day 7
KMT2A-rear.
NPM1
FLT3-ITD
DNMT3A
NRAS
TP53
BCR-ABL
MV4-11
MOLM13
CB MLL-AF9
OCI AML3
OCI AML2
IMS-M2
KG1A
K562
THP1
HL60
AUC
4
3
2
1
0
Genes
WT
Mut

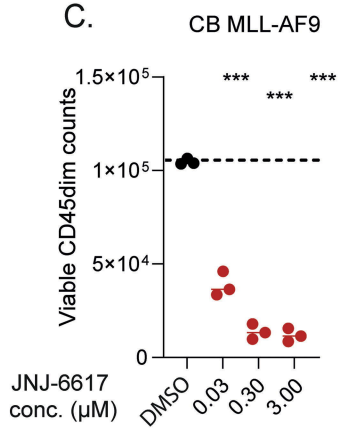
C.
CB MLL-AF9
Viable CD45dim counts
1.5×10^5
1×10^5
5×10^4
0
***
***
***
JNJ-6617 conc. (μM)
DMSO
0.03
0.30
3.00

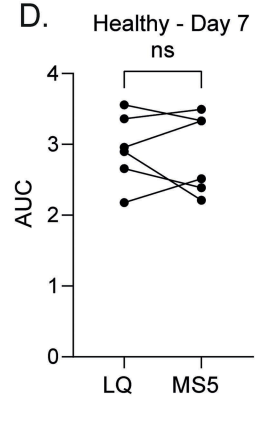
D.
Healthy - Day 7
ns
AUC
4
3
2
1
0
LQ
MS5

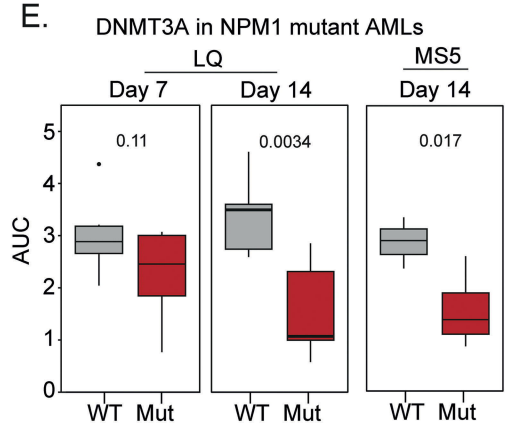
E.
DNMT3A in NPM1 mutant AMLs
LQ
MS5
Day 7
Day 14
Day 14
AUC
0.11
0.0034
0.017
WT
Mut
WT
Mut
WT
Mut

Figure 2

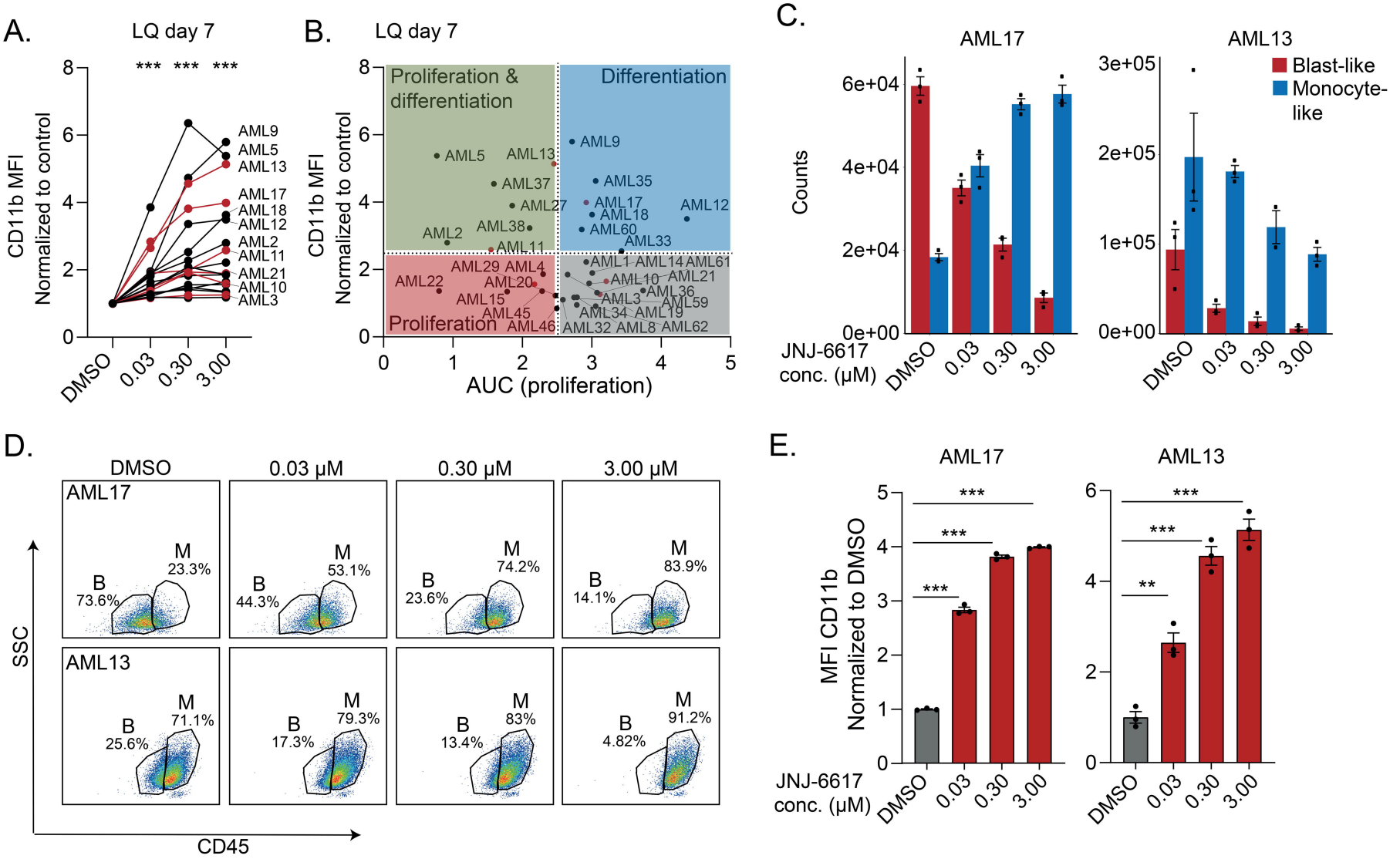
A.
LQ day 7
***
***
***
CD11b MFI
Normalized to control
AML9
AML5
AML13
AML17
AML18
AML12
AML2
AML11
AML21
AML10
AML3
DMSO
0.03
0.30
3.00
B.
LQ day 7
Proliferation &
differentiation
Differentiation
Proliferation
AML5
AML13
AML9
AML37
AML35
AML27
AML17
AML18
AML12
AML2
AML38
AML60
AML33
AML11
AML29
AML4
AML1
AML14
AML61
AML22
AML20
AML10
AML21
AML15
AML3
AML36
AML59
AML45
AML46
AML34
AML19
AML32
AML8
AML62
AUC (proliferation)
C.
AML17
AML13
Blast-like
Monocyte-
like
Counts
JNJ-6617
conc. (μM)
D.
DMSO
0.03 μM
0.30 μM
3.00 μM
AML17
AML13
B
M
73.6%
23.3%
44.3%
53.1%
23.6%
74.2%
14.1%
83.9%
25.6%
71.1%
17.3%
79.3%
13.4%
83%
4.82%
91.2%
SSC
CD45
E.
AML17
AML13
MFI CD11b
Normalized to DMSO
JNJ-6617
conc. (μM)

Figure 3

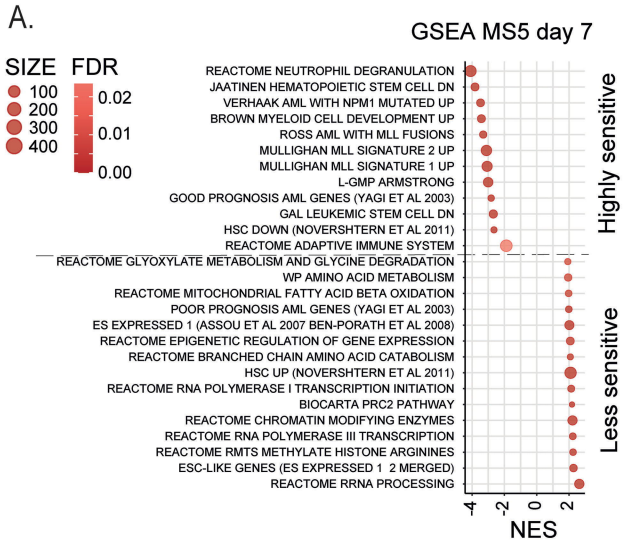
A.
GSEA MS5 day 7
SIZE
100
200
300
400
FDR
0.02
0.01
0.00
REACTOME NEUTROPHIL DEGRANULATION
JAATINEN HEMATOPOIETIC STEM CELL DN
VERHAAK AML WITH NPM1 MUTATED UP
BROWN MYELOID CELL DEVELOPMENT UP
ROSS AML WITH MLL FUSIONS
MULLIGHAN MLL SIGNATURE 2 UP
MULLIGHAN MLL SIGNATURE 1 UP
L-GMP ARMSTRONG
GOOD PROGNOSIS AML GENES (YAGI ET AL 2003)
GAL LEUKEMIC STEM CELL DN
HSC DOWN (NOVERSHTERN ET AL 2011)
REACTOME ADAPTIVE IMMUNE SYSTEM
REACTOME GLYOXYLATE METABOLISM AND GLYCINE DEGRADATION
WP AMINO ACID METABOLISM
REACTOME MITOCHONDRIAL FATTY ACID BETA OXIDATION
POOR PROGNOSIS AML GENES (YAGI ET AL 2003)
ES EXPRESSED 1 (ASSOU ET AL 2007 BEN-PORATH ET AL 2008)
REACTOME EPIGENETIC REGULATION OF GENE EXPRESSION
REACTOME BRANCHED CHAIN AMINO ACID CATABOLISM
HSC UP (NOVERSHTERN ET AL 2011)
REACTOME RNA POLYMERASE I TRANSCRIPTION INITIATION
BIOCARTA PRC2 PATHWAY
REACTOME CHROMATIN MODIFYING ENZYMES
REACTOME RNA POLYMERASE III TRANSCRIPTION
REACTOME RMTS METHYLATE HISTONE ARGININES
ESC-LIKE GENES (ES EXPRESSED 1 2 MERGED)
REACTOME RRNA PROCESSING
Highly sensitive
Less sensitive
-4
-2
0
2
NES

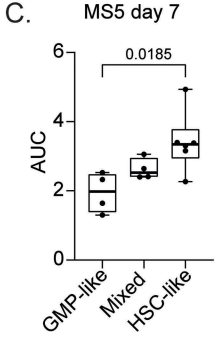
C.
MS5 day 7
0.0185
AUC
6
4
2
0
GMP-like
Mixed
HSC-like

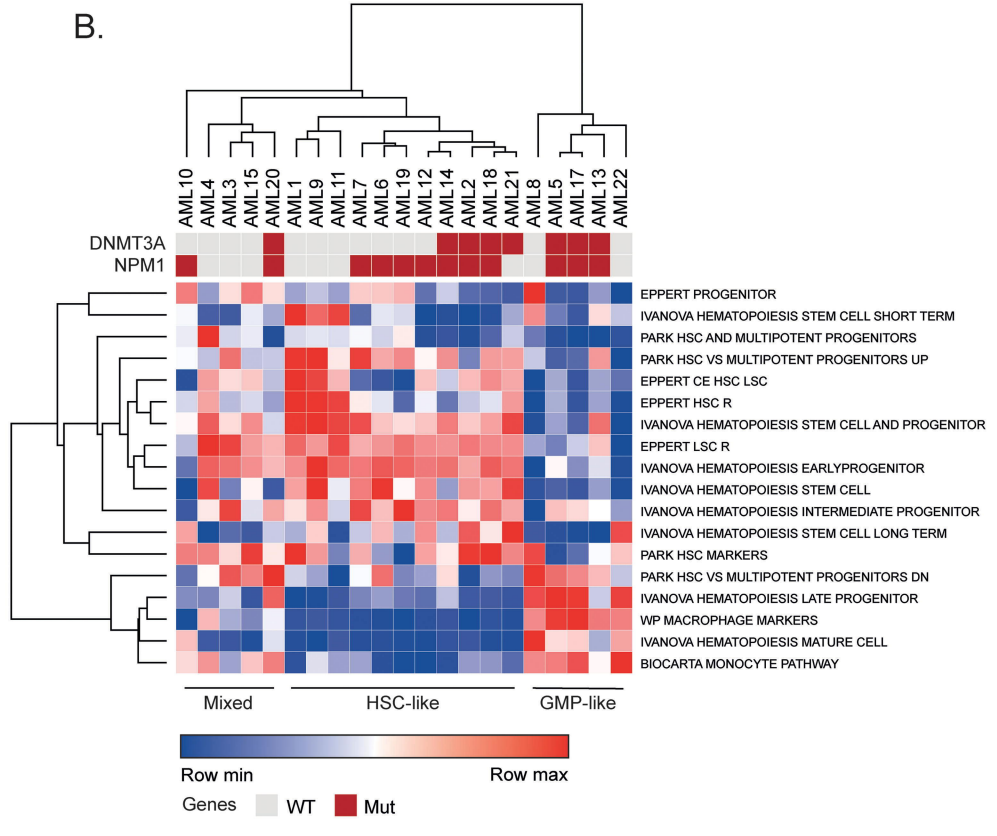
B.
AML10
AML4
AML3
AML15
AML20
AML1
AML9
AML11
AML7
AML6
AML19
AML12
AML14
AML2
AML18
AML21
AML8
AML5
AML17
AML13
AML22
DNMT3A
NPM1
EPPERT PROGENITOR
IVANOVA HEMATOPOIESIS STEM CELL SHORT TERM
PARK HSC AND MULTIPOTENT PROGENITORS
PARK HSC VS MULTIPOTENT PROGENITORS UP
EPPERT CE HSC LSC
EPPERT HSC R
IVANOVA HEMATOPOIESIS STEM CELL AND PROGENITOR
EPPERT LSC R
IVANOVA HEMATOPOIESIS EARLYPROGENITOR
IVANOVA HEMATOPOIESIS STEM CELL
IVANOVA HEMATOPOIESIS INTERMEDIATE PROGENITOR
IVANOVA HEMATOPOIESIS STEM CELL LONG TERM
PARK HSC MARKERS
PARK HSC VS MULTIPOTENT PROGENITORS DN
IVANOVA HEMATOPOIESIS LATE PROGENITOR
WP MACROPHAGE MARKERS
IVANOVA HEMATOPOIESIS MATURE CELL
BIOCARTA MONOCYTE PATHWAY
Mixed
HSC-like
GMP-like
Row min
Row max
Genes
WT
Mut

Figure 4

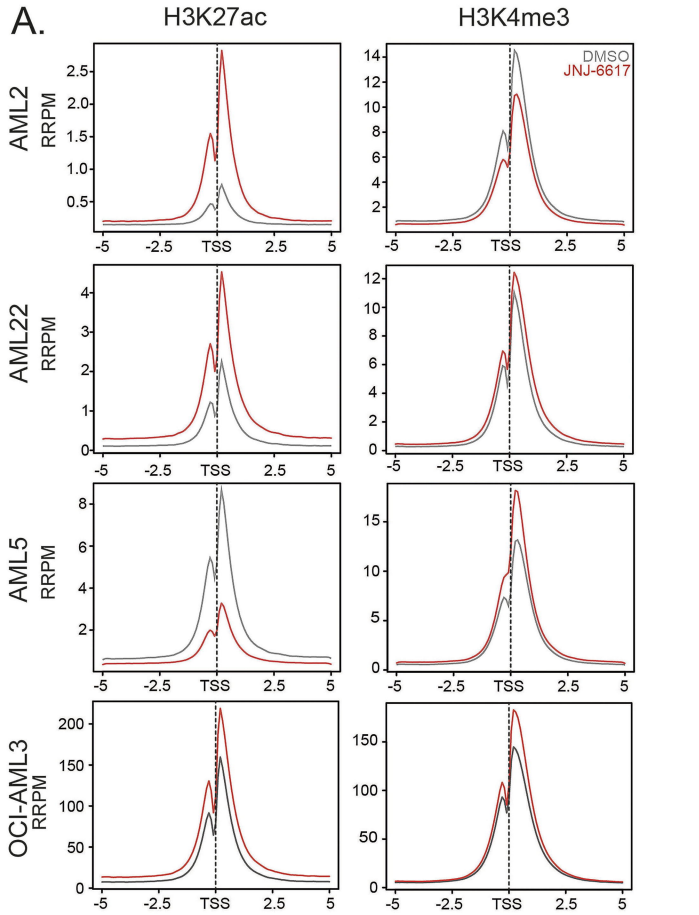
A.
H3K27ac
H3K4me3
DMSO
JNJ-6617
AML2
AML22
AML5
OCI-AML3
RRPM
-5
-2.5
TSS
2.5
5

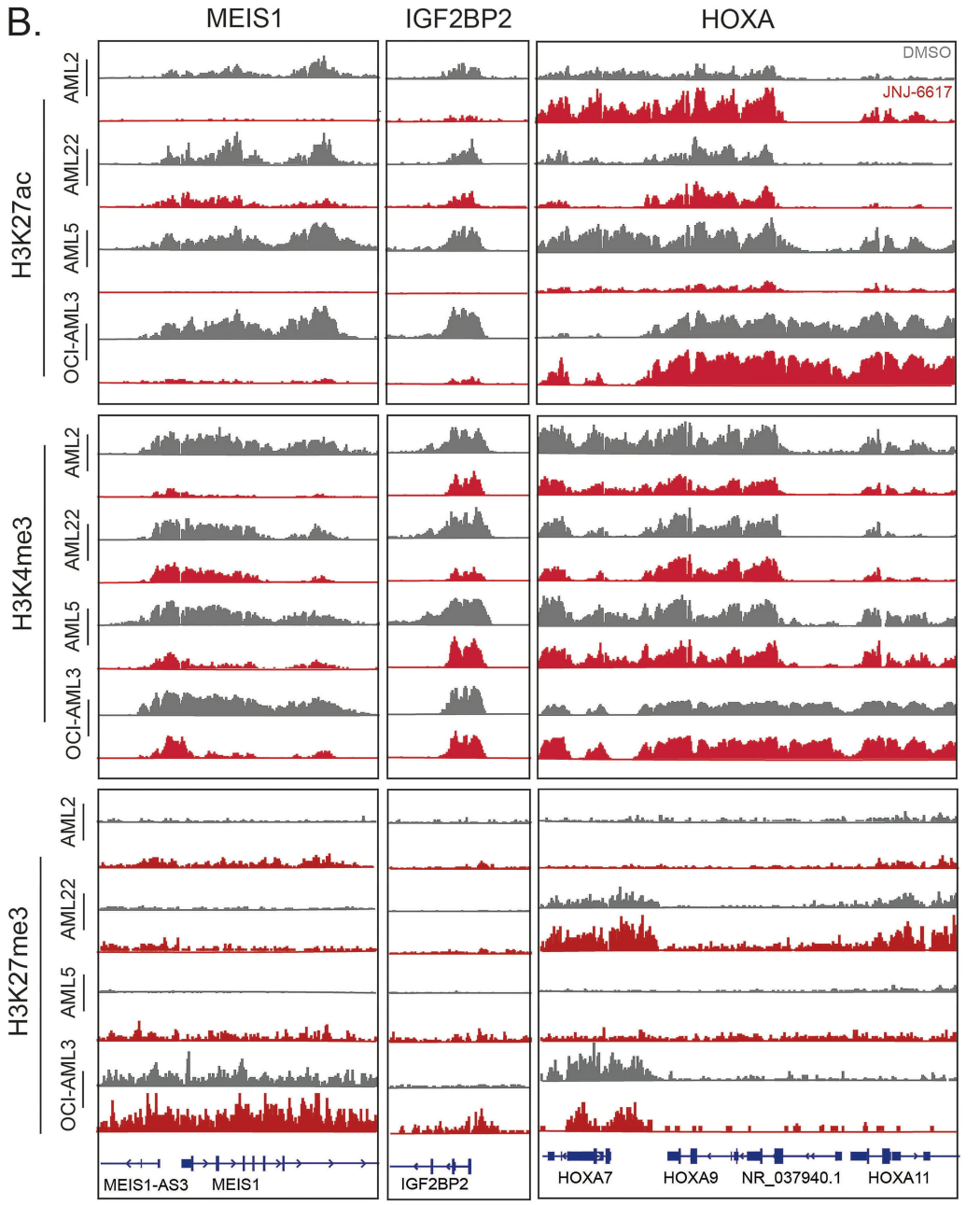
B.
MEIS1
IGF2BP2
HOXA
DMSO
JNJ-6617
H3K27ac
H3K4me3
H3K27me3
AML2
AML22
AML5
OCI-AML3
MEIS1-AS3
MEIS1
IGF2BP2
HOXA7
HOXA9
NR_037940.1
HOXA11

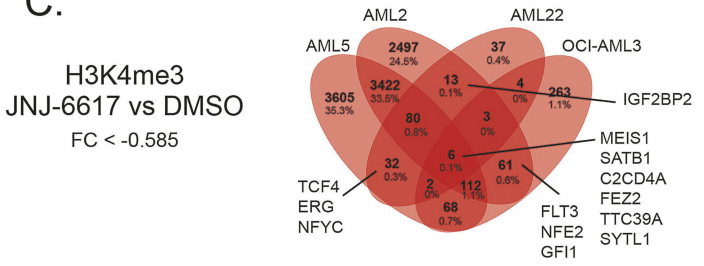
C.
H3K4me3
JNJ-6617 vs DMSO
FC < -0.585
AML2
AML22
AML5
OCI-AML3
IGF2BP2
2497
24.5%
37
0.4%
3605
35.3%
3422
33.5%
13
0.1%
4
0%
263
1.1%
80
0.8%
3
0%
6
0.1%
32
0.3%
61
0.6%
2
0%
112
1.1%
68
0.7%
MEIS1
SATB1
C2CD4A
FEZ2
TTC39A
SYTL1
TCF4
ERG
NFYC
FLT3
NFE2
GFI1

Figure 5

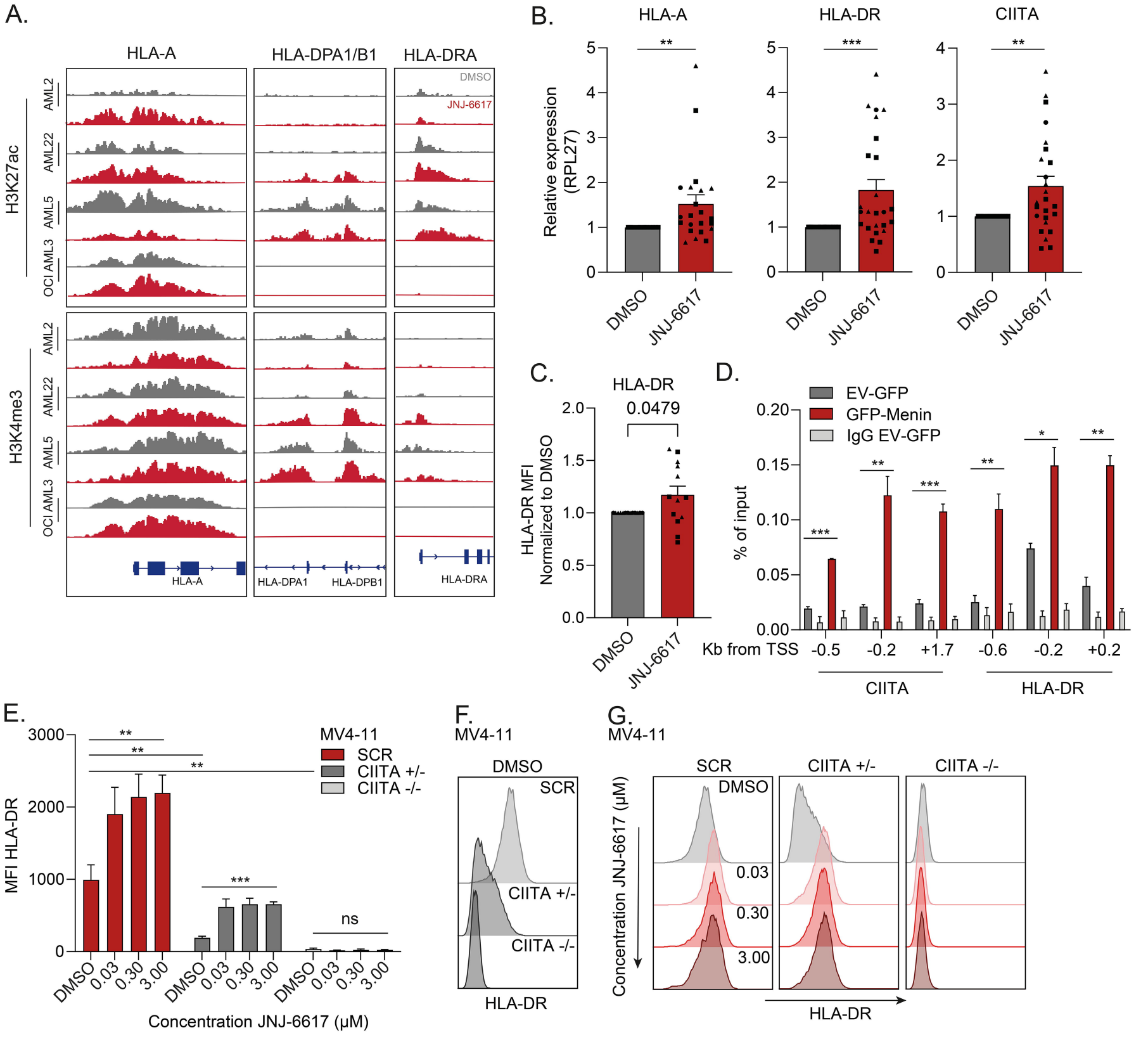
A.
HLA-A
HLA-DPA1/B1
HLA-DRA
DMSO
JNJ-6617
H3K27ac
H3K4me3
AML2
AML22
AML5
AML3
OCI
HLA-A
HLA-DPA1
HLA-DPB1
HLA-DRA
B.
HLA-A
HLA-DR
CIITA
Relative expression (RPL27)
DMSO
JNJ-6617
C.
HLA-DR
0.0479
HLA-DR MFI Normalized to DMSO
D.
EV-GFP
GFP-Menin
IgG EV-GFP
% of input
Kb from TSS
-0.5
-0.2
+1.7
-0.6
-0.2
+0.2
CIITA
HLA-DR
E.
MV4-11
SCR
CIITA +/-
CIITA -/-
MFI HLA-DR
Concentration JNJ-6617 (μM)
ns
F.
MV4-11
DMSO
SCR
CIITA +/-
CIITA -/-
HLA-DR
G.
MV4-11
SCR
CIITA +/-
CIITA -/-
DMSO
0.03
0.30
3.00
Concentration JNJ-6617 (μM)
HLA-DR

Figure 6

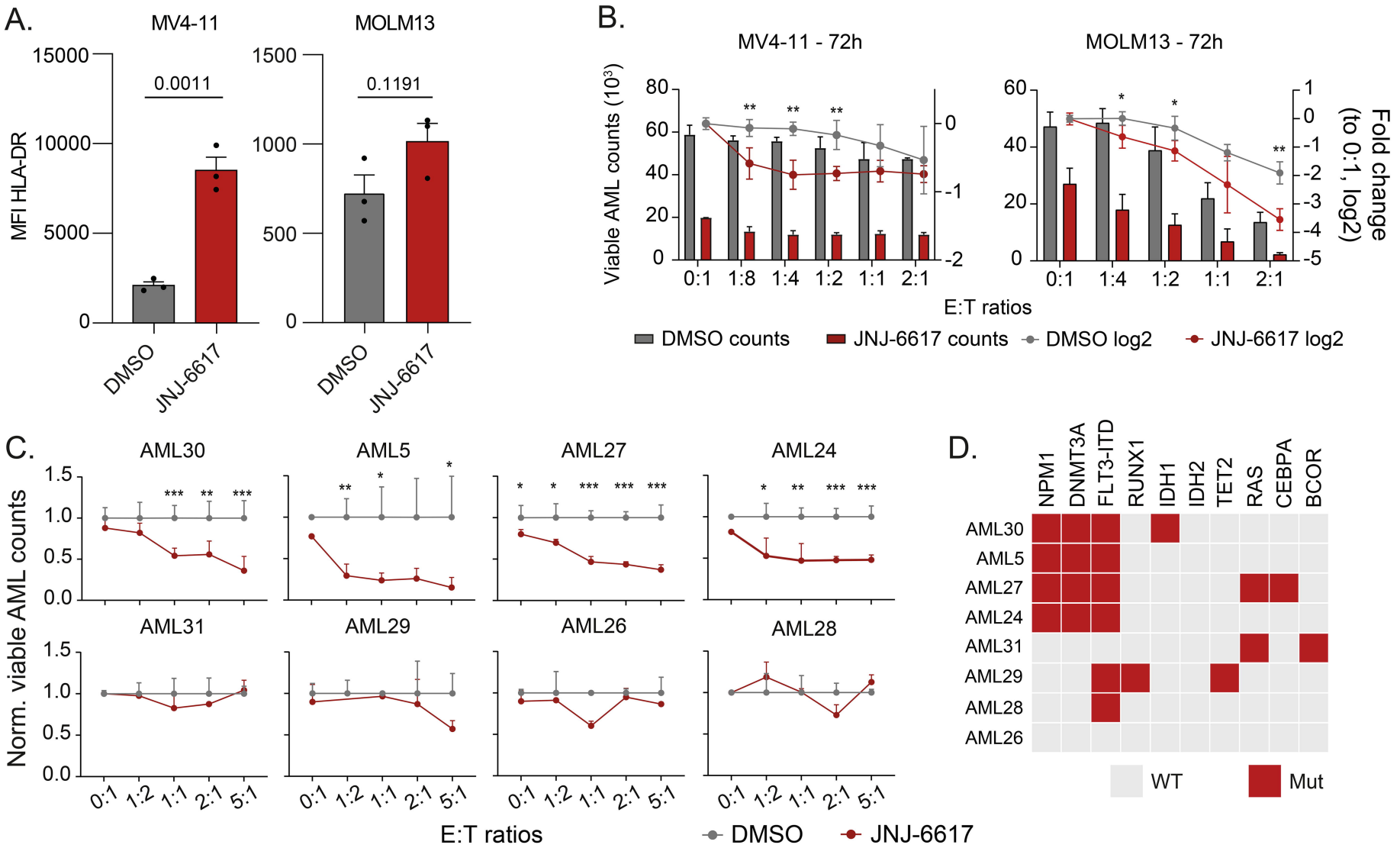
A.
MV4-11
MOLM13
MFI HLA-DR
0.0011
0.1191
DMSO
JNJ-6617
B.
MV4-11 - 72h
MOLM13 - 72h
Viable AML counts (10³)
Fold change (to 0:1, log2)
E:T ratios
DMSO counts
JNJ-6617 counts
DMSO log2
JNJ-6617 log2
C.
AML30
AML5
AML27
AML24
AML31
AML29
AML26
AML28
Norm. viable AML counts
E:T ratios
DMSO
JNJ-6617
D.
NPM1
DNMT3A
FLT3-ITD
RUNX1
IDH1
IDH2
TET2
RAS
CEBPA
BCOR
WT
Mut

Figure 7

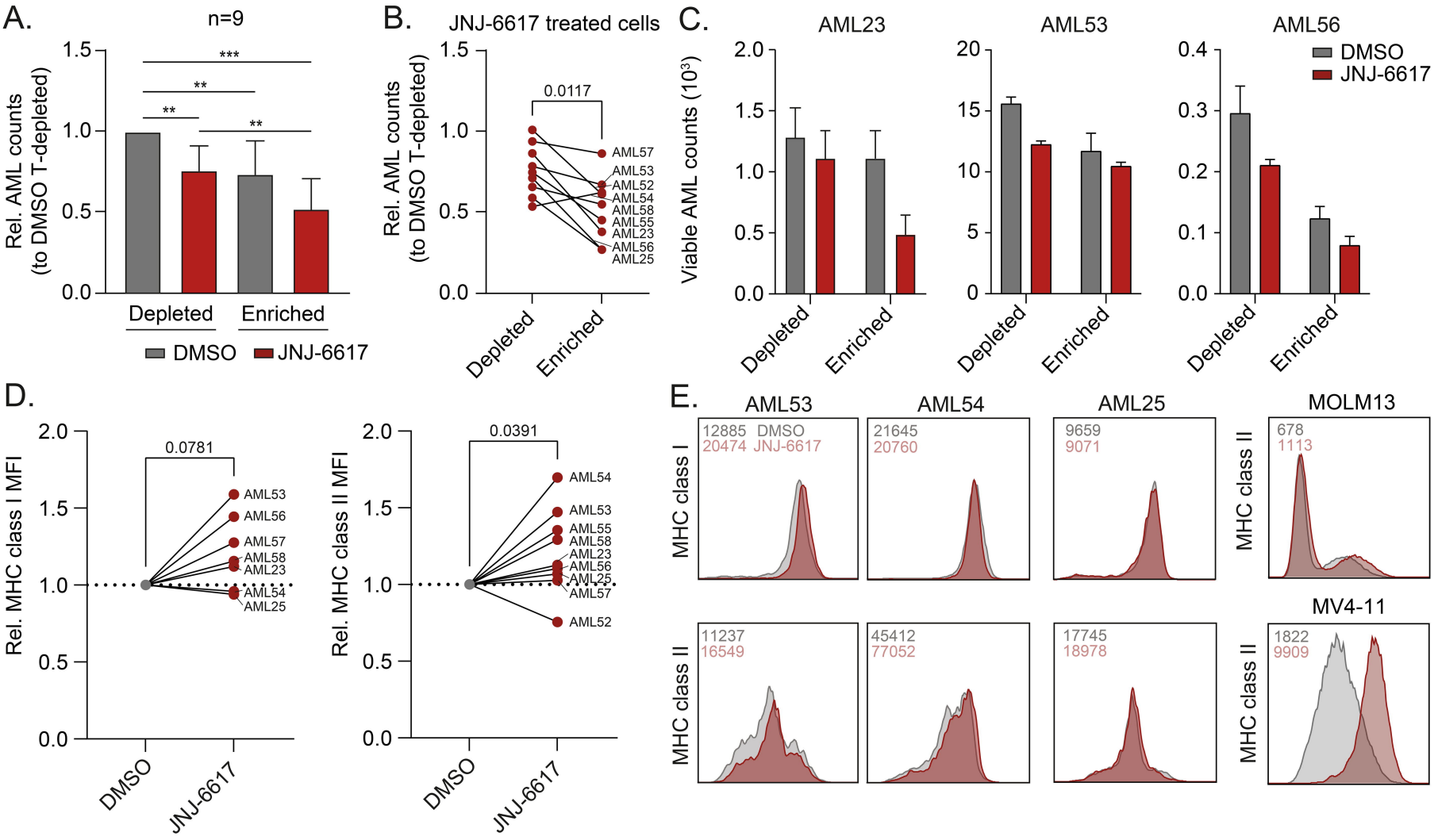
A.
n=9
Rel. AML counts (to DMSO T-depleted)
1.5
1.0
0.5
0.0
***
**
**
**
Depleted
Enriched
DMSO
JNJ-6617
B.
JNJ-6617 treated cells
Rel. AML counts (to DMSO T-depleted)
0.0117
AML57
AML53
AML52
AML54
AML58
AML55
AML23
AML56
AML25
Depleted
Enriched
C.
AML23
AML53
AML56
Viable AML counts (10³)
DMSO
JNJ-6617
Depleted
Enriched
D.
Rel. MHC class I MFI
0.0781
AML53
AML56
AML57
AML58
AML23
AML54
AML25
DMSO
JNJ-6617
Rel. MHC class II MFI
0.0391
AML54
AML53
AML55
AML58
AML23
AML56
AML25
AML57
AML52
E.
AML53
AML54
AML25
MOLM13
MV4-11
MHC class I
MHC class II
12885 DMSO
20474 JNJ-6617
21645
20760
9659
9071
678
1113
11237
16549
45412
77052
17745
18978
1822
9909

Supplemental Figures and Methods

Bleximenib, the novel menin-KMT2A inhibitor JNJ-75276617, impairs long-term proliferation and immune evasion in acute myeloid leukemia

Shanna M. Hogeling[1], Duy Minh Le[1], Nikita La Rose[1], Min Chul Kwon[2], Albertus T.J. Wierenga[1], Fiona A.J. van den Heuvel[1], Vincent van den Boom[1], Anna Kuchnio[2], Ulrike Philippar[2], Gerwin Huls[1] and Jan Jacob Schuringa[1*]

[1]Department of Hematology, University Medical Center Groningen, University of Groningen, Groningen, The Netherlands; [2]Discovery Oncology, Janssen R&D, Beerse, BE

Supplemental figure 1

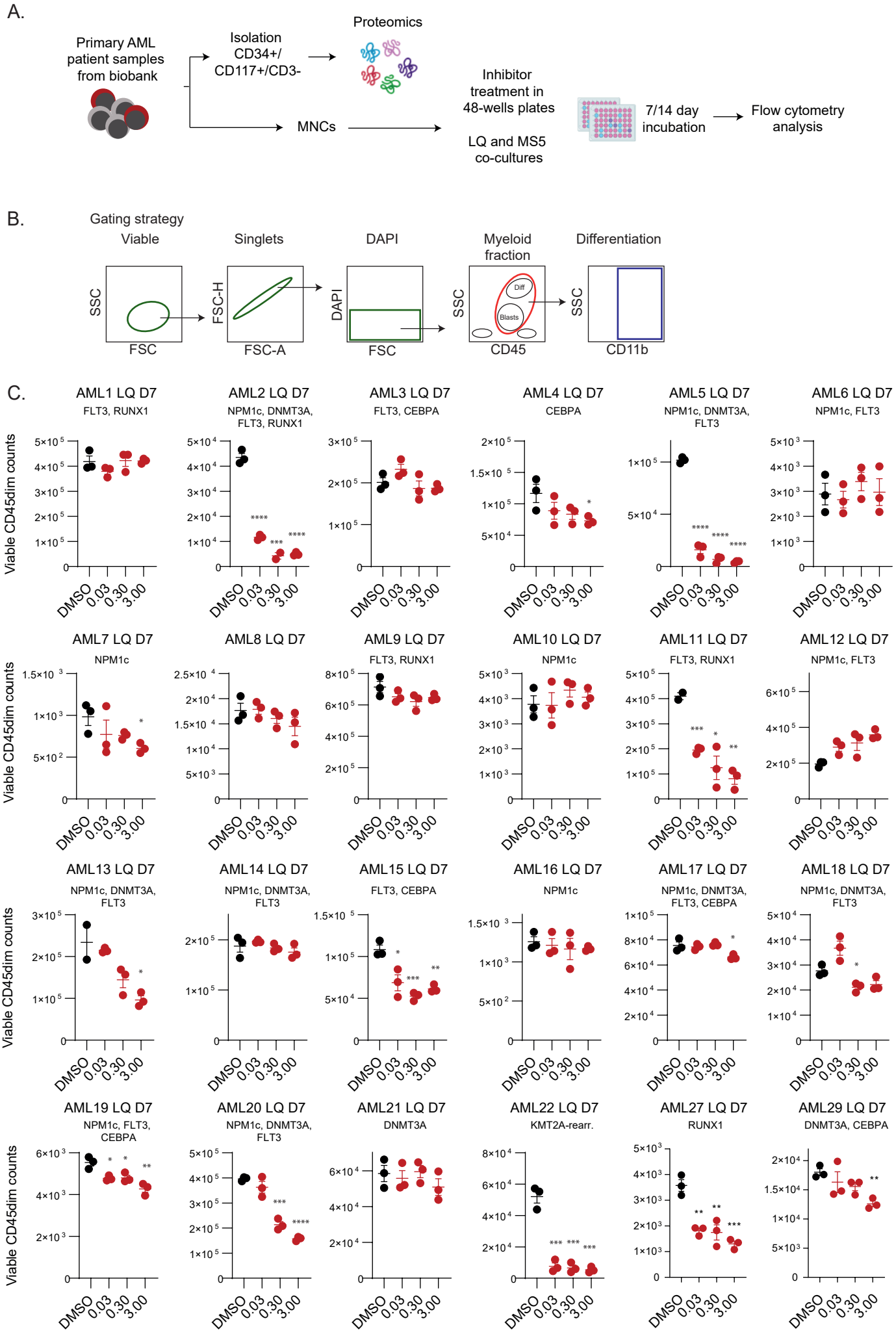

Supplemental figure 1 - continued

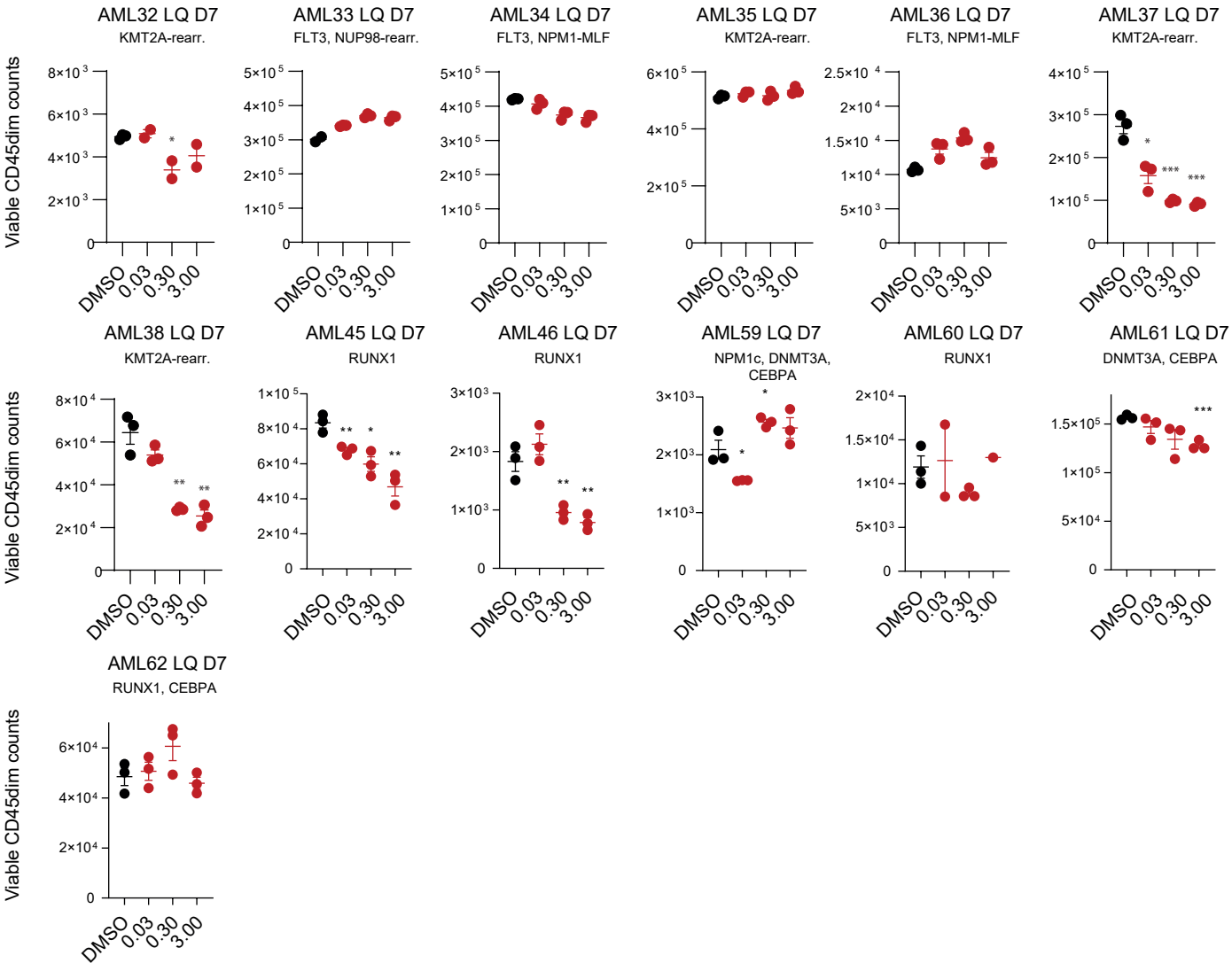

Supplemental figure 2

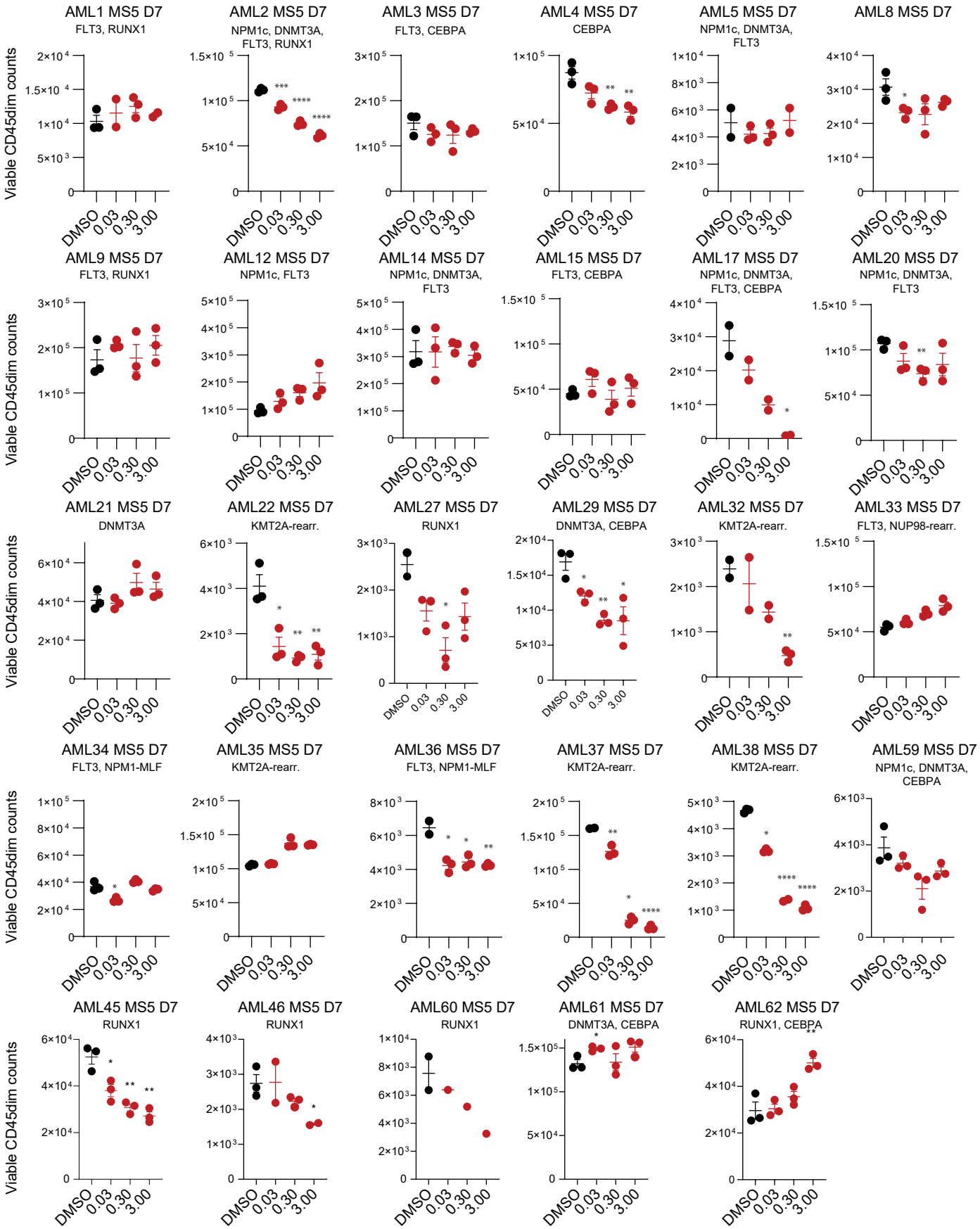

Supplemental figure 3

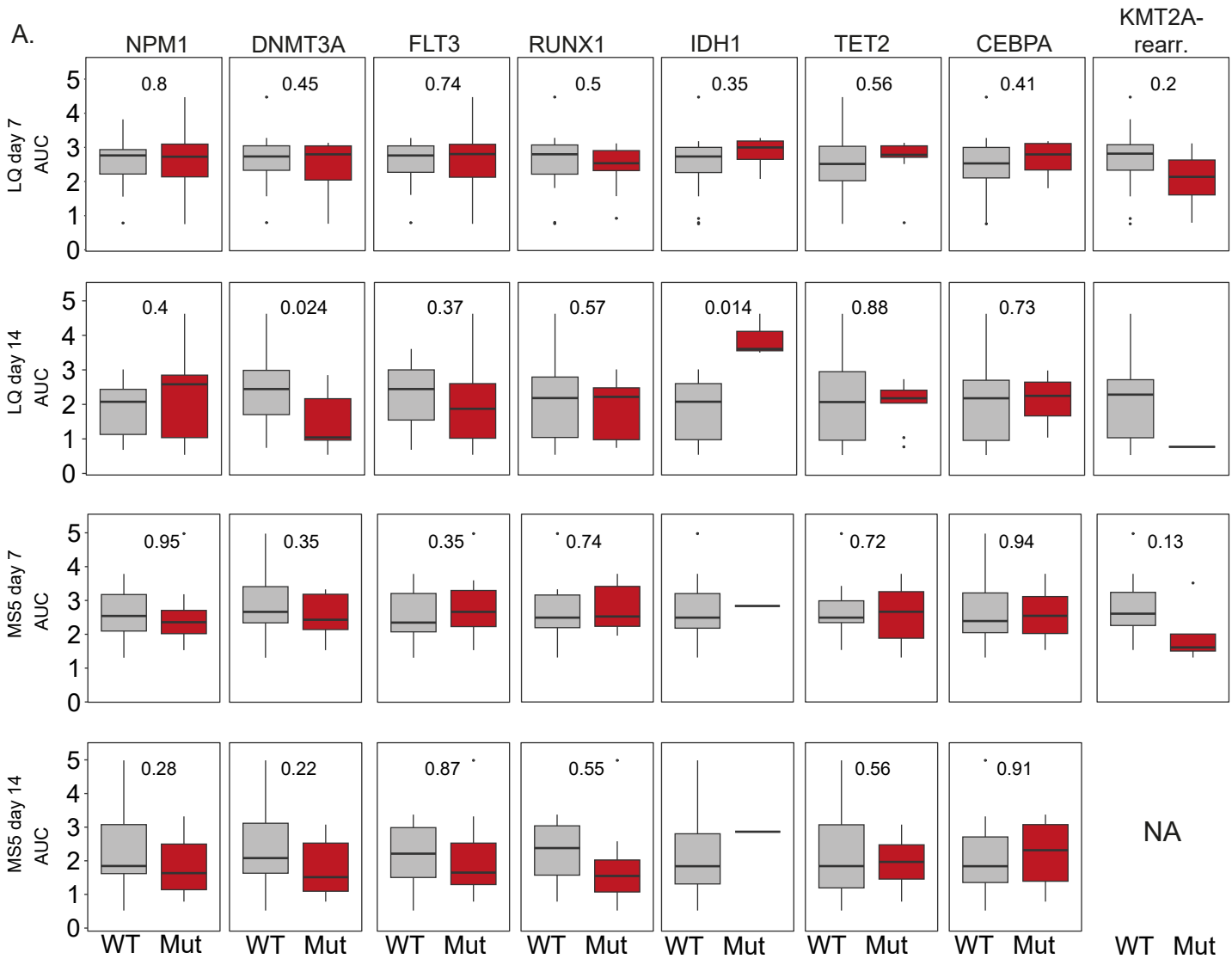

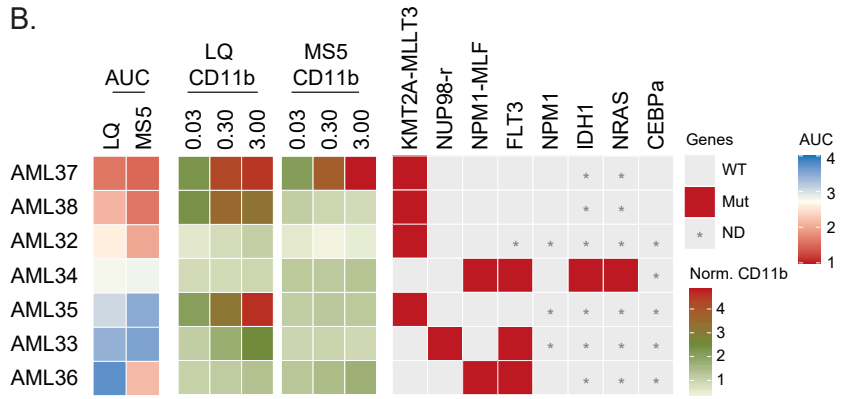

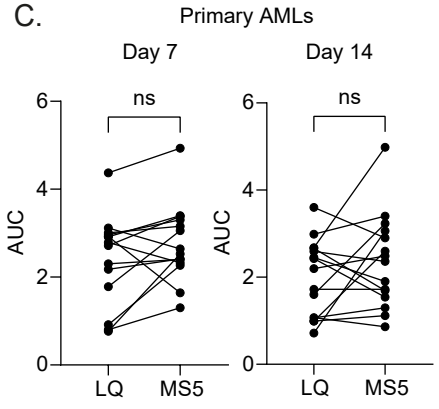

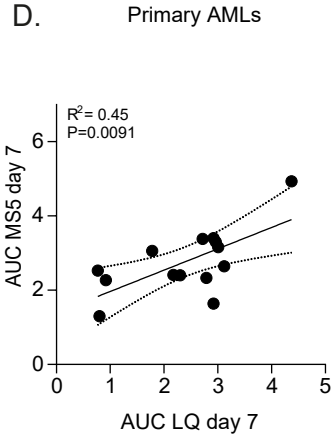

Supplemental figure 4

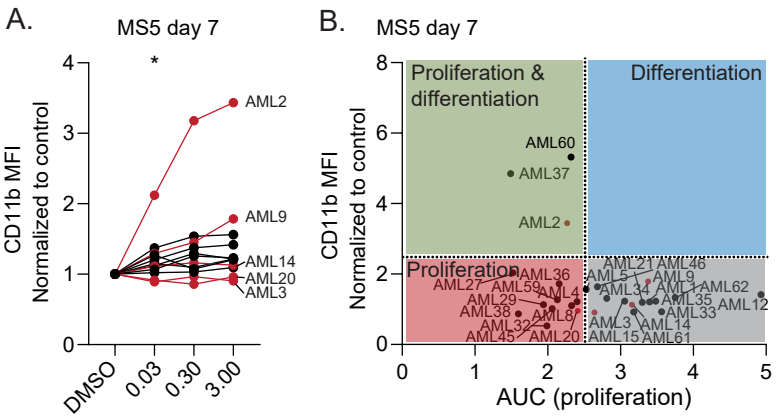

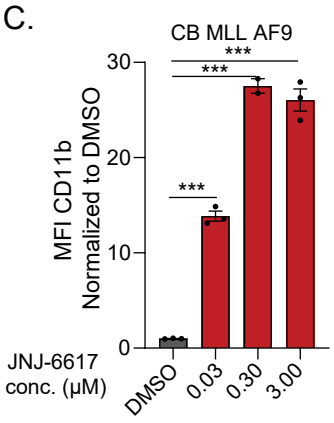

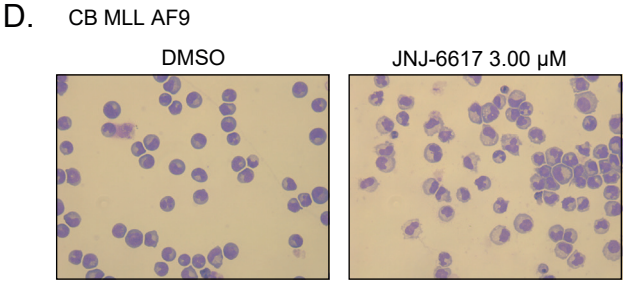

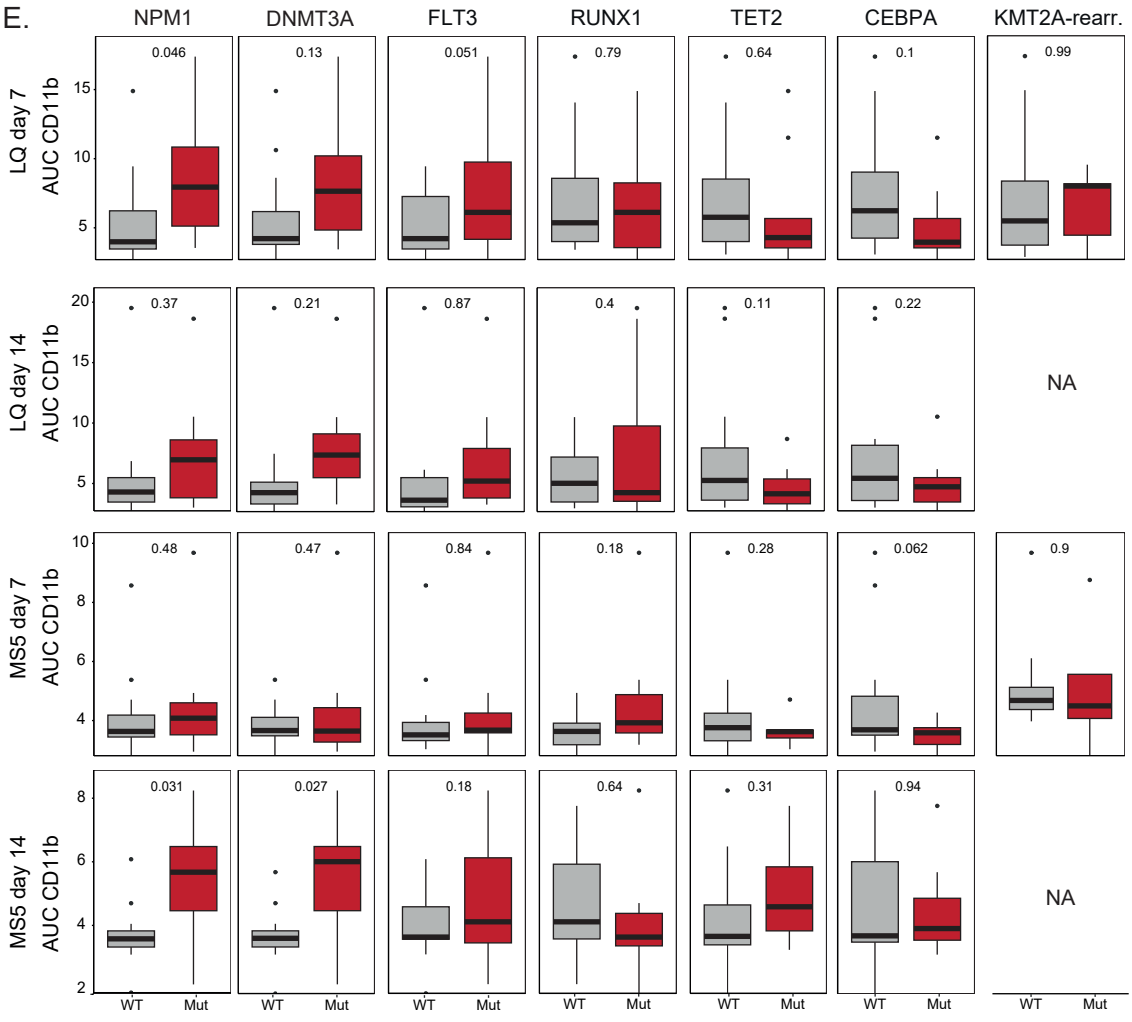

Supplemental figure 5

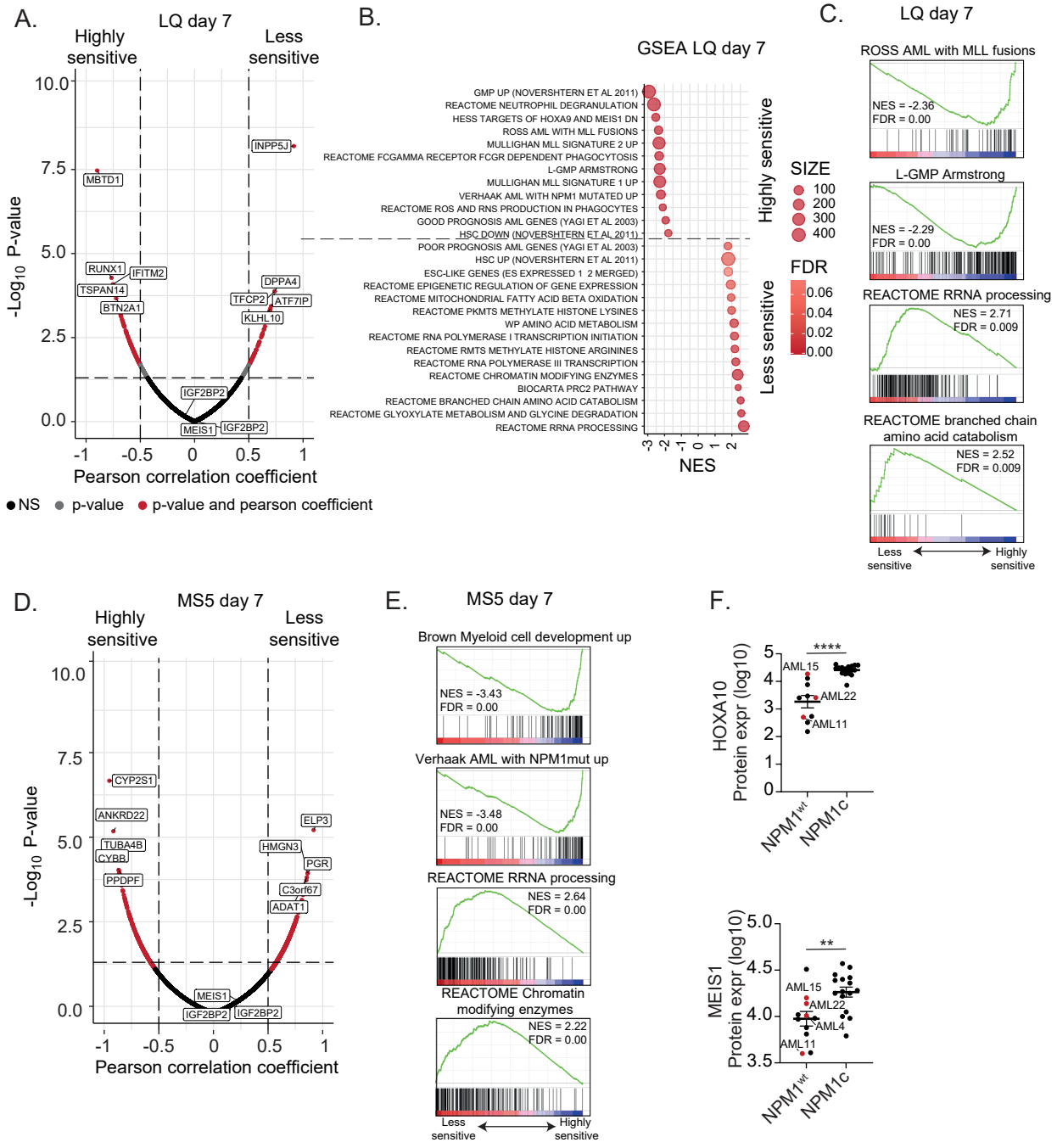

Supplemental figure 6

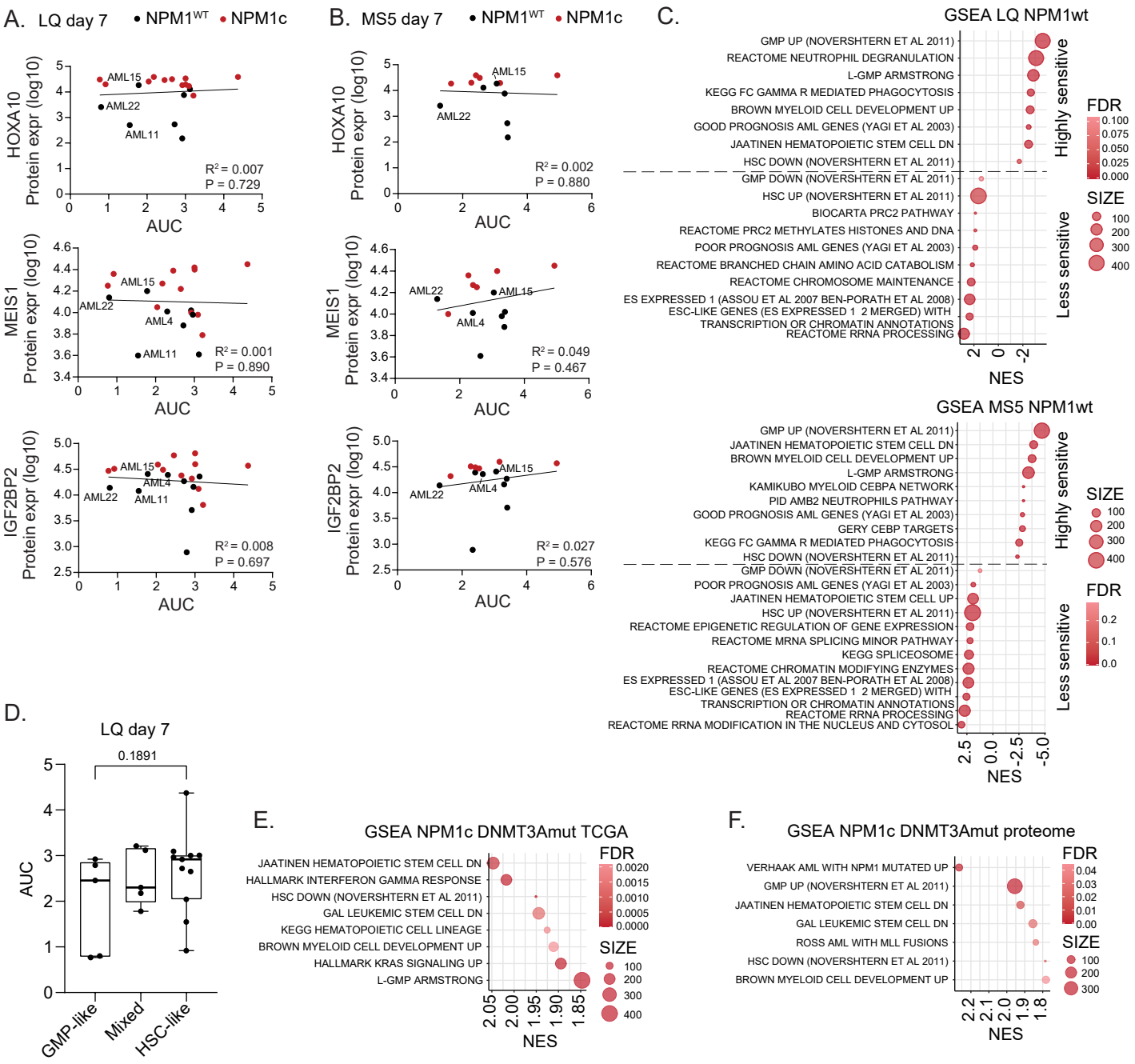

Supplemental figure 7

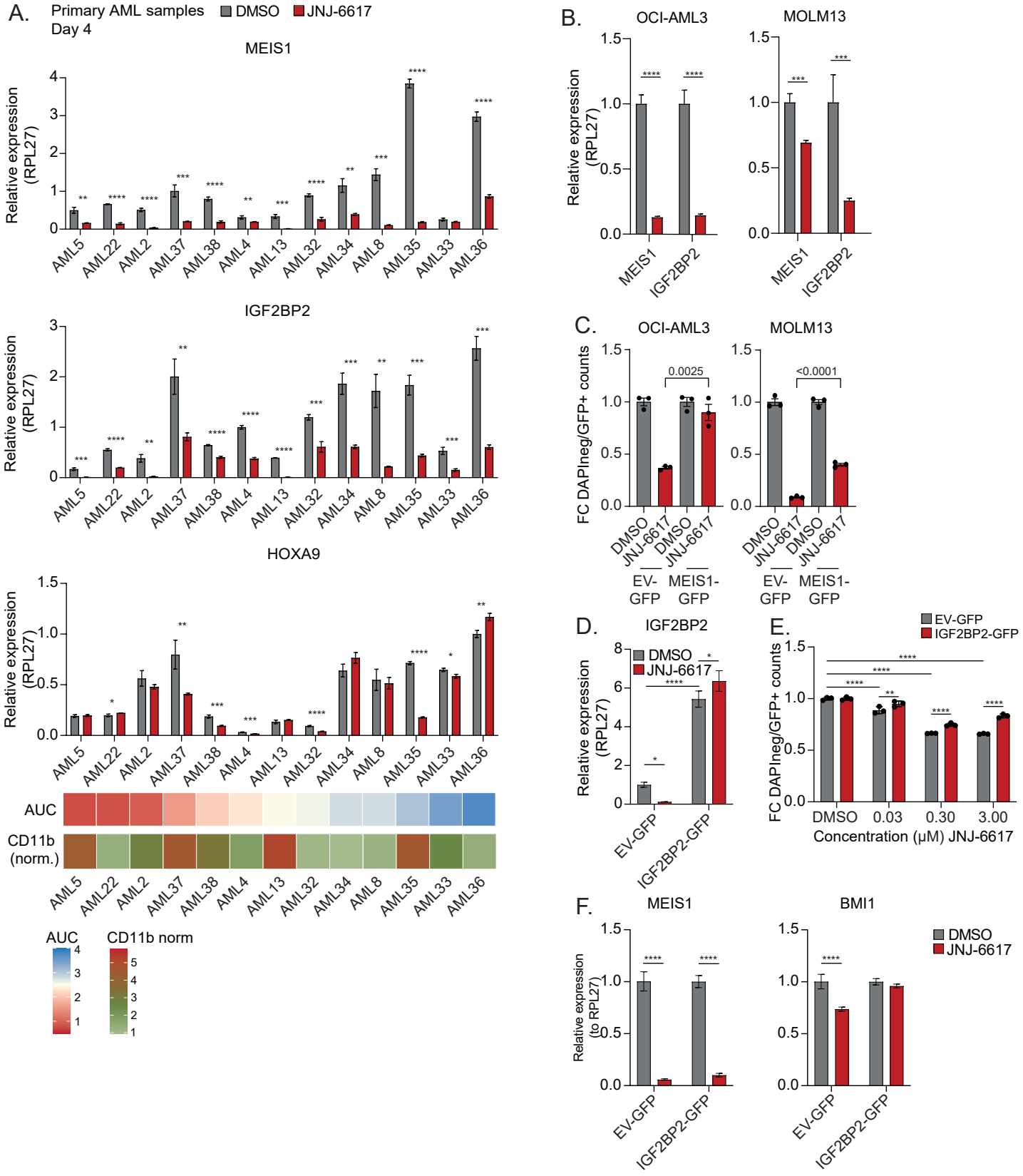

Supplemental figure 8

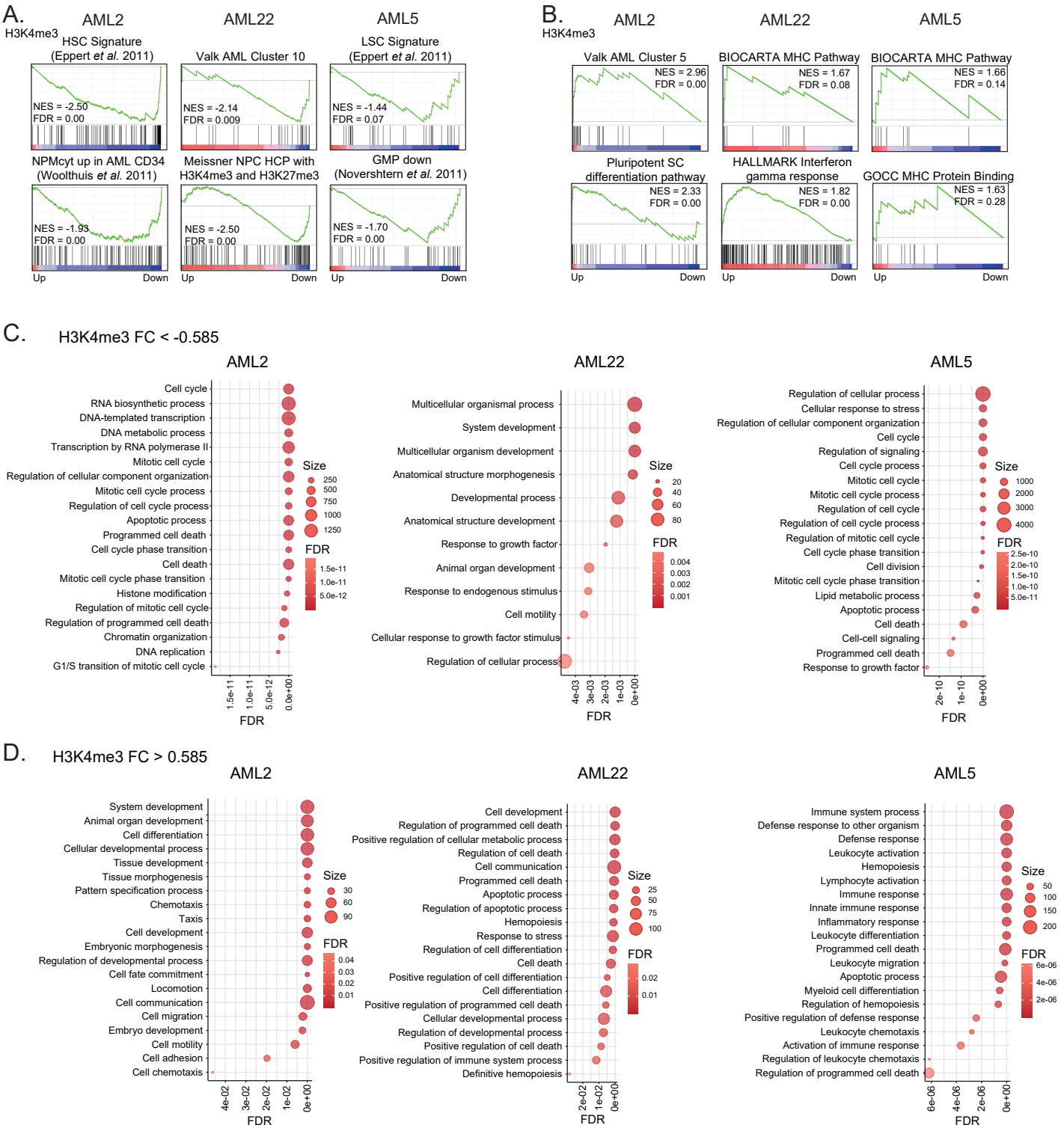

Supplemental figure 9

A. H3K27ac FC > 0.585

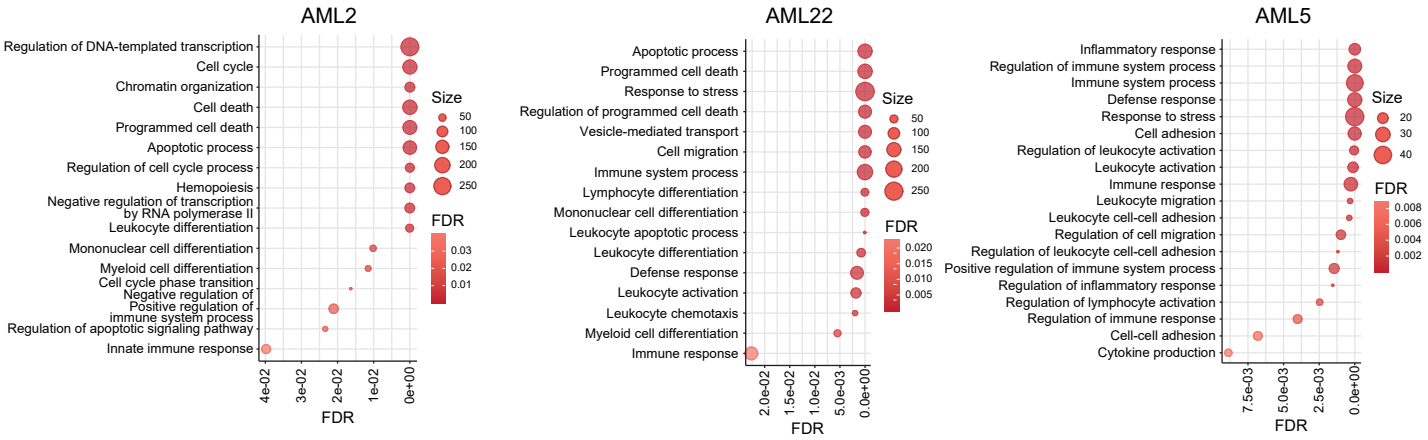

B. GSEA analysis H3K4me3 OCI-AML3 FC > 0.585

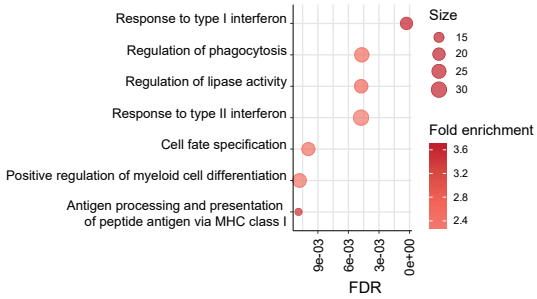

Supplemental figure 10

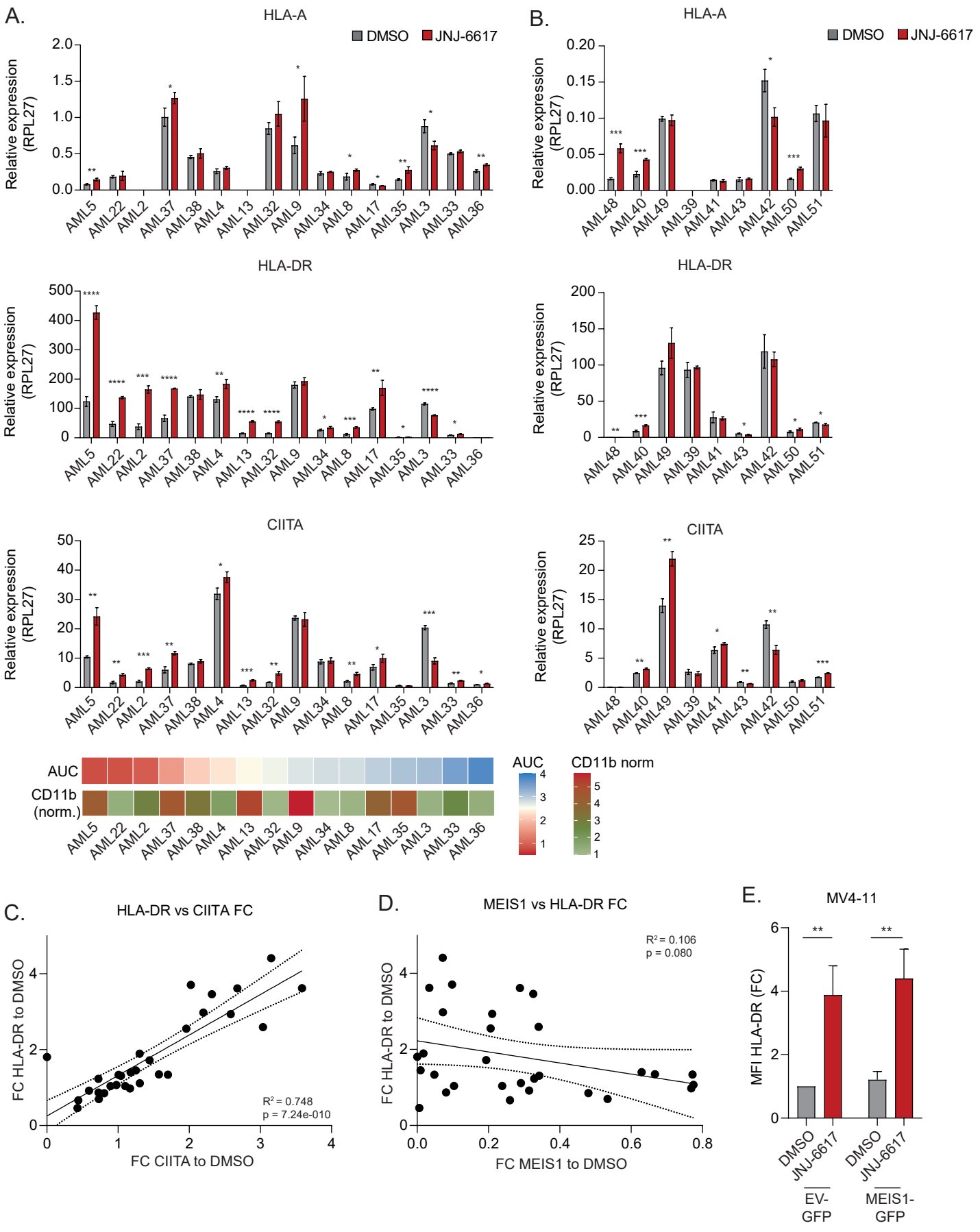

Supplemental figure 11

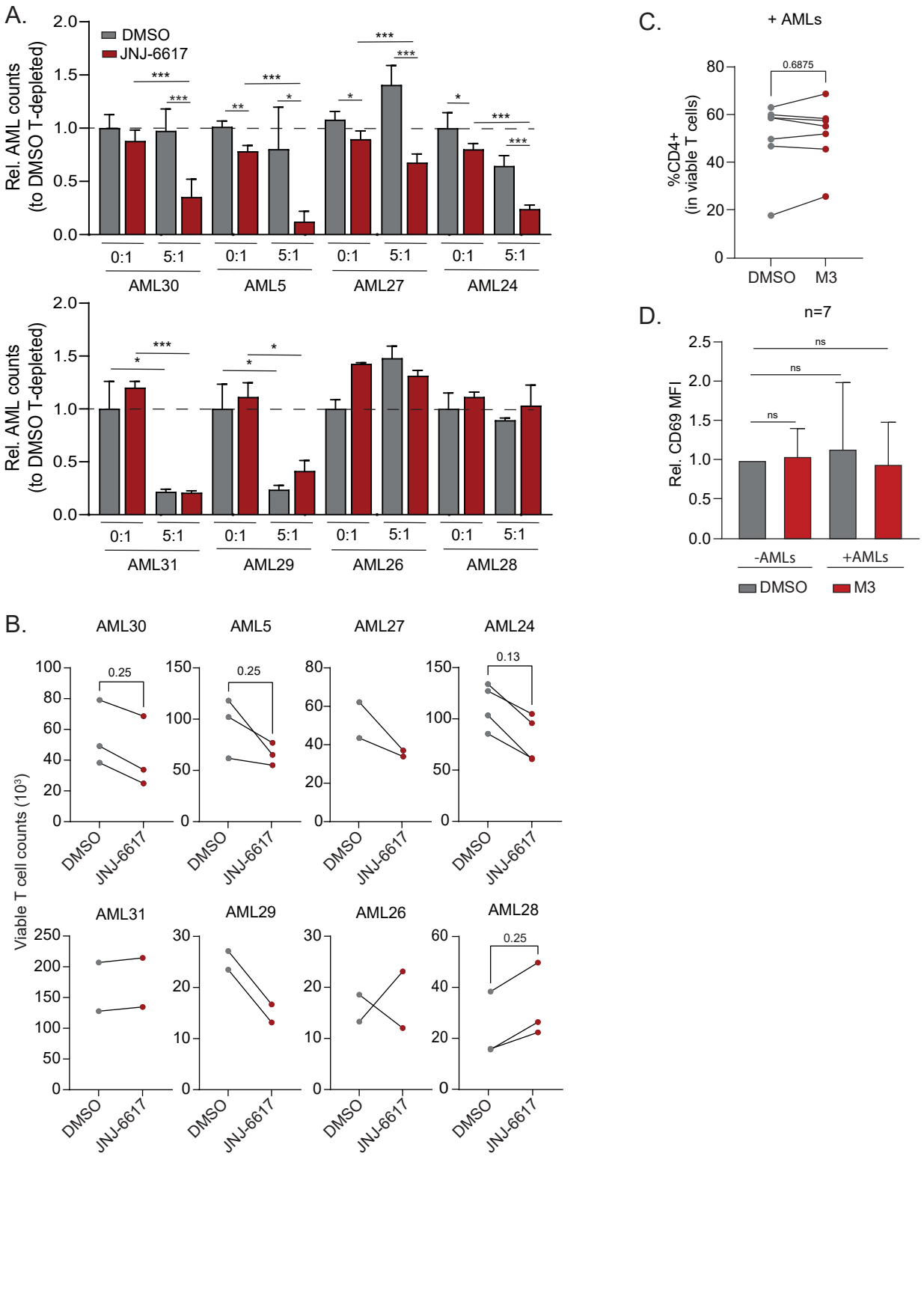

Supplemental table 1. AML studies used in the study

		Mutations																			AUC							FC compared to DMSO T-depleted		FC compared to DMSO T-depleted		FC compared to DMSO (MFI)			FC compared to DMSO (mRNA expression)						
AML	material	FLT3	NPM	DNMT3A	IDH1/2	TET2	ASXL1	RAS	WT1	RUNX1	CKIT	Splicing SF3B1, SRSF2	CEBPA	EZH2	U2AF1	BCOR/BCORL1	ANKRD26	MYC	GATA2	karyotype	LQ 7	LQ 14	MSS 7	MSS 14	ChIPseq	LFQ proteome	T-cell killing assay	FC T-cell killing 0:1	FC T-cell killing 5:1	FC T-cell killing (depleted)	FC T-cell killing (enriched)	MHC class I (HLA-A/B/C)	MHC class II (HLA-DR/DQ/DP)	HLA-DR	MEIS1	IGF2BP2	HOXA9	HLA-A	HLA-DR	CIITA
AML1	PB	0.1 (c.17	wt	wt	wt	wt	wt	wt	wt	0.44 (c.72	wt	wt	wt	wt	wt	wt	wt	wt	wt	NK	2.9	2.7	3.4	5.0		yes															
AML2	PB	ITD	0.5	0.5	wt	wt	wt	wt	wt	0.55 (c.72	wt	wt	wt	wt	wt	wt	wt	wt	wt	wt	NK	0.9	1.0	2.3	1.1	yes	yes								1.487179	0.07	0.03	0.86		4.41	3.15
AML3	BM	0.35 (c.1	wt	wt	wt	wt	wt	wt	wt	wt	wt	wt	0.5 (c.89	wt	wt	wt	wt	wt	wt	wt	NK	3.1	1.7	2.6	1.7		yes										0.26	0.30		0.70	0.66	0.44
AML4	PB	wt	wt	wt	wt	wt	wt	wt	wt	wt	0.23 (c.2	wt	0.05 (c.5	wt	wt	wt	wt	wt	wt	wt	inv16	2.3	3.0	2.4	3.4		yes								1.5822	0.63	0.38	0.55	1.19	1.40	1.18
AML5	BM	0.3 (c.17	0.36 (c.8	0.48 (c.2	wt	wt	wt	wt	wt	wt	wt	wt	wt	wt	wt	wt	wt	wt	wt	wt	NK	0.8	0.6	2.5		yes	yes	allogenic	0.78	0.12							0.33	0.06	1.02	1.83	3.46	2.32
AML6	PB	0.51 (c.1	0.43 (c.8	wt	0.34 (IDH	wt	wt	wt	wt	wt	wt	wt	wt	wt	wt	wt	wt	wt	wt	wt	NK	3.1	4.6				yes															
AML7	BM	wt	0.42 (c.8	wt	0.34 (IDH	wt	wt	wt	wt	wt	wt	wt	wt	wt	wt	wt	wt	wt	wt	wt	nd	2.0	3.6		2.9		yes															
AML8	BM	wt	wt	wt	wt	wt	wt	wt	wt	wt	wt	mut	wt	wt	wt	wt	wt	wt	wt	wt	NK	2.8	2.5	2.3	1.9		yes										0.07	0.13	0.95	1.52	2.98	2.20
AML9	PB	0.12 (c.2	wt	wt	wt	0.32 (c.3	0.31 (c.1	wt	wt	0.48 (c.4	wt	wt	wt	0.99 (c.2	wt	wt	wt	wt	wt	wt	nd	2.7	2.4	3.4	1.5		yes										0.78	0.33		2.02	1.07	0.98
AML10	PB	wt	0.38 (c.8	wt	0.35 (IDH	wt	wt	wt	wt	wt	wt	wt	wt	wt	wt	wt	wt	wt	wt	wt	nd	3.2	3.5				yes															
AML11	PB	ITD	wt	wt	wt	wt	0.5 (c.20	wt	wt	0.98 (c.4	wt	wt	wt	0.98 (c.2	wt	wt	wt	wt	wt	wt	nd	1.5	0.8				yes															
AML12	PB	ITD	0.38 (c.8	wt	wt	wt	wt	wt	wt	wt	wt	wt	wt	wt	wt	wt	wt	wt	wt	wt	nd	4.4	10.0	4.9	3.3		yes															
AML13	PB	0.27	0.42 (c.8	0.48 (c.2	wt	wt	wt	wt	wt	wt	wt	wt	wt	wt	wt	wt	wt	wt	wt	wt	nd	2.5	1.0		2.6		yes								1.154255	0.03	0.06	1.14	4.60	3.62	3.59
AML14	BM	ITD	0.37 (c.8	0.4 (c.26	wt	0.3 (c.51	wt	wt	wt	wt	wt	wt	wt	wt	wt	wt	wt	wt	wt	wt	NK 46,XY[20]	3.0	2.2	3.2	2.5		yes															
AML15	BM	ITD	wt	wt	wt	wt	wt	wt	wt	wt	wt	wt	mut	wt	wt	wt	wt	wt	wt	wt	46,XX,t(11;17)(p15;q21)[10]	1.8	1.6	3.1	3.2		yes															
AML16	BM	wt	0.33	wt	wt	0.42	wt	wt	0.05	wt	wt	wt	wt	wt	wt	wt	wt	wt	wt	wt	nd	2.7	2.7																			
AML17	PB	0.29 (c.1	0.38 (c.8	0.42 (c.2	wt	0.51 (c.5	wt	wt	wt	wt	wt	wt	mut	wt	wt	wt	wt	wt	wt	wt	46,XX	2.9	1.1	1.6	0.9		yes								0.19			0.75	1.72	1.44
AML18	PB	0.15 (c.2	0.36 (c.8	0.43 (c.2	wt	wt	wt	wt	0.44 (c.1	wt	wt	wt	wt	wt	wt	wt	wt	wt	wt	wt	46,XX	3.0	2.7		1.7		yes															
AML19	PB	0.2 (c.17	0.39 (c.8	wt	wt	0.51 (c.3	wt	wt	wt	wt	wt	wt	mut	wt	wt	wt	wt	wt	wt	wt	46,XX	2.7	2.6		2.4		yes															
AML20	BM	0.32 (c.1	0.38 (c.8	0.47 (c.2	wt	wt	wt	wt	wt	wt	mut	wt	wt	wt	wt	wt	wt	wt	wt	wt	46,XX	2.2	1.1	2.4	1.3		yes															
AML21	BM	wt	wt	0.47 (c.2	0.49 (IDH	wt	wt	0.44 (NR/	wt	wt	wt	0.03 (SF3	wt	wt	wt	wt	wt	wt	wt	wt	47,XX,+8[12]/45,XX,-7[4]/46,XX[1	3.0	0.7	3.3	3.1		yes															
AML22	PB	wt	wt	wt	wt	0.03 (c.3	wt	wt	wt	wt	wt	0.52 (SR	wt	wt	wt	wt	wt	wt	wt	wt	6,XY,t(11;22)(q23;q13)[10]/46,XY[12] KMT2A-EP300	0.8	0.8	1.3		yes	yes									0.34	0.06	1.12	1.03	2.94	2.58
AML23	BM	wt	cyt	nd	nd	nd	nd	nd	nd	nd	nd	nd	nd	nd	nd	nd	nd	nd	nd	nd	NK							autologous			0.87	0.38	1.13	1.12							
AML24	BM	ITD	0.43	0.36	wt	wt	wt	wt	wt	wt	wt	wt	wt	wt	wt	wt	wt	wt	wt	wt	NK							allogenic	0.90	0.68					1.445135							
AML25	BM	ITD	cyt	nd	nd	nd	nd	nd	nd	nd	nd	nd	nd	nd	nd	nd	nd	nd	nd	nd	NK							autologous			0.59	0.27	1.07	0.94							
AML26	BM	wt	wt	wt	wt	wt	wt	wt	wt	wt	wt	wt	wt	wt	wt	wt	wt	wt	wt	wt	NK							allogenic	1.43	1.31												
AML27	BM	0.26, 0.12	0.43	0.43	wt	wt	wt	0.05 (KR/	wt	wt	wt	wt	mut	wt	wt	wt	wt	wt	wt	wt	nd	1.8	2.9	1.5	1.0			allogenic	0.80	0.24					1.348404							
AML28	BM	ITD	wt	wt	wt	wt	wt	wt	wt	wt	wt	wt	wt	wt	wt	wt	wt	wt	wt	wt	+8							allogenic	1.11	1.03												
AML29	BM	0.44	wt	wt	wt	0.48	wt	wt	wt	0.48	wt	wt	wt	wt	wt	wt	wt	wt	wt	wt	NK	2.5	2.1	1.9	1.7			allogenic	1.11	0.41												
AML30	PB	0.47	0.48	0.48	0.43	wt	wt	wt	wt	wt	wt	wt	wt	wt	wt	wt	wt	wt	wt	wt	NK							allogenic	0.88	0.35												
AML31	BM	wt	wt	wt	wt	wt	wt	mut	wt	wt	wt	wt	wt	wt	wt	wt	wt	wt	wt	wt	NK							allogenic	1.20	0.21												
AML32	PB	nd	nd	nd	nd	nd	nd	nd	nd	nd	nd	nd	nd	nd	nd	nd	nd	nd	nd	nd	46,XX,t(9;11)(p22;q23)	2.6		2.0												0.29	0.51	0.42	1.23	3.61	2.68
AML33	PB	ITD	nd	nd	nd	nd	nd	nd	nd	nd	nd	nd	nd	nd	nd	nd	nd	nd	nd	nd	46,XY,t(7;11)(p15;p15)	3.4		3.6												0.77	0.29	0.90	1.06	1.34	1.70
AML34	BM	0.73	wt	wt	0.34	wt	wt	0.03	wt	wt	wt	wt	wt	wt	wt	nd	nd	nd	nd	nd	47,XY,t(3;5)(q23;q33),+8[10]	2.8		2.8												0.34	0.33	1.20	1.09	1.31	1.04
AML35	BM	wt	nd	nd	nd	nd	nd	nd	nd	nd	nd	nd	nd	nd	nd	nd	nd	nd	nd	nd	46,XX,t(9;11)(p22;q23)[8]	3.1		3.5												0.05	0.24	0.25	1.89	1.34	1.01
AML36	PB	ITD	wt	nd	nd	nd	nd	nd	nd	nd	nd	nd	nd	nd	nd	nd	nd	nd	nd	nd	6,XX,t(3;5)(q23;q33)[7]/46,XX[3]	3.7		2.2												0.29	0.24	1.17	1.34	1.12	1.31
AML37	BM	wt	wt	nd	nd	nd	nd	nd	nd	nd	nd	nd	wt	nd	nd	nd	nd	nd	nd	nd	46,XY,t(9;11)(p22;q23)	1.6		1.5												0.21	0.41	0.52	1.27	2.55	1.96
AML38	BM	wt	wt	nd	nd	nd	nd	nd	nd	nd	nd	nd	wt	nd	nd	nd	nd	nd	nd	nd	46,XX,t(9;11)(p22;q23)	2.1		1.6												0.24	0.63	0.51	1.10	1.04	1.10
AML39	PB	0.23	wt	0.45	wt	0.5	wt	0.06	wt	wt	wt	0.34	wt	wt	wt	wt	wt	wt	wt	wt	46,XX,t(10;17;15;21)(p11;q27?4;q15;q22)[4]/ 46,XX,t(1;12)(p13;p1															0.10	0.17	0.26		1.04	0.89
AML40	BM	ITD	cyt	nd	nd	nd	nd	nd	nd	nd	nd	nd	nd	nd	nd	nd	nd	nd	nd	nd	nd															0.10	0.03		1.90	3.71	2.02
AML41	BM	wt	wt	wt	wt	wt	wt	0.48	wt	wt	wt	wt	wt	wt	wt	0.05	wt	wt	wt	wt	t(3,12)															0.77			0.92	0.98	1.17
AML42	BM	ITD	wt	wt	wt	wt	wt	wt	wt	wt	wt	wt	wt	wt	wt	wt	wt	wt	wt	wt	+8															0.31			0.67	0.92	0.59
AML43	PB	wt	wt	wt	wt	wt	wt	wt	wt	wt	wt	wt	wt	wt	wt	wt	wt	wt	wt	wt	45,XY,-7,del(12)(p11p12)[7]/46,XY[3]															0.53	0.40	0.38	1.09	0.70	0.73
AML45	PB	wt	wt	wt	wt	wt	0.43	wt	wt	0.59	0.22	wt	wt	wt	wt	wt	wt	wt	wt	wt	47XY,+21	2.277	3.02	2.058	1.9																	
AML46	PB	wt	wt	wt	wt	wt	wt	wt	wt	0.44	wt	wt	wt	wt	wt	wt	wt	wt	wt	wt	6,XY,?inv(2)(p?21q?21),del(5)(p13p15),-7[10]	2.487		2.685	1.15																			
AML48	PB	ITD	wt	nd	nd	nd	nd	nd	nd	nd	pos	nd	nd	nd	nd	nd	nd	nd	nd	nd	complex															0.20	0.07	0.09	3.61	0.46	0.43
AML49	PB	wt	cyt	nd	nd	nd	nd	nd	nd	nd	nd	nd	nd	nd	nd	nd	nd	nd	nd	nd	NK															0.67	0.25		0.98	1.35	1.57
AML50	PB	0.26 (c.1	0.36 (c.8	0.49 (c.2	0.12 (IDH	wt	wt	wt	wt	wt	wt	wt	wt	wt	wt	wt	wt	wt	wt	wt	46, XY													0.988189	0.01	0.03	0.63	1.87	1.45	1.25
AML51	PB	nd	nd	nd	nd	nd	nd	nd	nd	nd	nd	nd	nd	nd	nd	nd	nd	nd	nd	nd	nd															0.08	0.21	0.72	0.90	0.87	0.73
AML52	BM	wt	cyt	nd	nd	nd	nd	nd	nd	nd	nd	nd	nd	nd	nd	nd	nd	nd	nd	nd	NK							autologous			1.01	0.61	0.76		0.961165						
AML53	BM	wt	cyt	nd	nd	nd	nd	nd	nd	nd	nd	nd	nd	nd	nd	nd	nd	nd	nd	nd	complex							autologous			0.79	0.67	1.47	1.59							
AML54	BM	0.13	0.4	0.5	0.4	wt	wt	wt	wt	wt	wt	wt	wt	wt	wt	wt	wt	wt	wt	wt	NK							autologous			0.54	0.62	1.70	0.96	1.12037						
AML55	PB	wt	cyt	nd	nd	nd	nd	nd	nd	nd	nd	nd	nd	nd	nd	nd	nd	nd	nd	nd	NK							autologous			0.75	0.45	1.36								
AML56	PB	wt	cyt	nd	nd	nd	nd	nd	nd	nd	nd	nd	nd	nd	nd	nd	nd	nd	nd	nd	NK							autologous			0.71	0.27	1.10	1.44							
AML57	BM	wt	cyt	nd	nd	nd	nd	nd	nd	nd	nd	nd	nd	nd	nd	nd	nd	nd	nd	nd	NK							autologous			0.94	0.86	1.03	1.28							
AML58	PB	ITD	cyt	nd	nd	nd	nd	nd	nd	nd	nd	nd	mut	nd	nd	nd	nd	nd	nd	nd	NK							autologous			0.66	0.55	1.29	1.16							
AML59	PB	wt		0.43	0.51	wt	0.46	wt	wt	0.06, 0.1	wt	wt	wt	0.31	wt	wt	wt	wt	wt	wt	NK	3.072		2.126	1.46																	
AML60	PB	wt		wt	wt	wt	wt	0.32(NR/	0.32 (c.13	0.43 (c.85	wt	wt	wt	0.48 (c.47	0.45 (BCC	0.34 (c.2	0.48 (c.13	9T>C)		NK	2.847	1.01	2.322	0.6																			
AML61	BM	wt		wt	0.48	wt	0.36	wt	wt	wt	wt	0.44, 0.0	wt	wt	wt	wt	wt	wt	wt	wt	NK	2.742	2.13	3.181	3.11																	
AML62	BM	wt		wt	wt	wt	0.47	wt	wt	wt	0.02	wt	0.55 (SR	0.34	wt	wt	wt	wt	wt	0.23	NK	3.052	2.4	3.753	2.62																	

Supplemental table 2. GSEA terms

Supplemental Table 2. GSEA terms					
follow link to MSigDB	**SIZE**	**ES**	**NES**	**NOM p-val**	**FDR q-val**
AML 2					
HSC SIGNATURE (EPPERT ET AL 2011)	86	-0.44	-2.50	0.00	0.00
LSC SIGNATURE (EPPERT 2011)	32	-0.29	-1.20	0.20	0.25
VALK_AML_CLUSTER_10	ns				
NPMCYT UP IN AML CD34 (WOOLTHUIS ET AL 2011)	94	-0.33	-1.93	0.00	0.00
MEISSNER_NPC_HCP_WITH_H3K4ME3_AND_H3K27ME3	101	-0.34	-1.92	0.00	0.07
GMP_DOWN (NOVERSHTERN ET AL 2011)	37	-0.32	-1.47	0.07	0.09
REACTOME_TRANSCRIPTIONAL_REGULATION_OF_PLURIP(	17	-0.64	-2.35	0.00	0.00
VALK_AML_CLUSTER_5	25	0.53	2.96	0.00	0.00
HALLMARK_INTERFERON_GAMMA_RESPONSE	ns				
GOCC_MHC_CLASS_I_PROTEIN_COMPLEX	5	0.54	1.46	0.04	0.36
BIOCARTA_MHC_PATHWAY	10	0.49	1.89	0.00	0.06
GOMF_MHC_PROTEIN_BINDING	19	0.30	1.60	0.08	0.27
AML 22					
HSC SIGNATURE (EPPERT ET AL 2011)	ns				
LSC SIGNATURE (EPPERT 2011)	ns				
VALK_AML_CLUSTER_10	25	-0.47	-2.14	0.00	0.01
NPMCYT UP IN AML CD34 (WOOLTHUIS ET AL 2011)	ns				
MEISSNER_NPC_HCP_WITH_H3K4ME3_AND_H3K27ME3	96	-0.33	-2.50	0.00	0.00
GMP_DOWN (NOVERSHTERN ET AL 2011)	ns				
REACTOME_TRANSCRIPTIONAL_REGULATION_OF_PLURIP(	17	0.64	1.59	0.01	0.11
VALK_AML_CLUSTER_5	29	0.56	1.62	0.02	0.10
HALLMARK_INTERFERON_GAMMA_RESPONSE	170	0.50	1.82	0.00	0.00
GOCC_MHC_CLASS_II_PROTEIN_COMPLEX	7	0.97	2.05	0.00	0.00
REACTOME_MHC_CLASS_II_ANTIGEN_PRESENTATION	98	0.46	1.62	0.00	0.10
BIOCARTA_MHC_PATHWAY	10	0.70	1.67	0.00	0.08
GOMF_MHC_PROTEIN_BINDING	17	0.71	1.94	0.00	0.01
AML 5					
HSC SIGNATURE (EPPERT ET AL 2011)	84	-0.39	-1.28	0.07	0.24
LSC SIGNATURE (EPPERT 2011)	31	-0.48	-1.44	0.01	0.07
VALK_AML_CLUSTER_10	27	-0.55	-1.72	0.00	0.05
NPMCYT UP IN AML CD34 (WOOLTHUIS ET AL 2011)	ns				
MEISSNER_NPC_HCP_WITH_H3K4ME3_AND_H3K27ME3	91	-0.48	-1.63	0.00	0.11
GMP_DOWN (NOVERSHTERN ET AL 2011)	37	-0.55	-1.70	0.00	0.00
REACTOME_TRANSCRIPTIONAL_REGULATION_OF_PLURIP(	18	-0.51	-1.45	0.02	0.29
VALK_AML_CLUSTER_5	ns				
HALLMARK_INTERFERON_GAMMA_RESPONSE	ns				
GOCC_MHC_CLASS_II_PROTEIN_COMPLEX	7	0.50	1.48	0.05	0.36
BIOCARTA_MHC_PATHWAY	10	0.51	1.66	0.00	0.14
GOMF_MHC_PROTEIN_BINDING	12	0.50	1.63	0.08	0.28

Supplemental Figure Legends

Supplemental figure 1. JNJ-75276617 impairs long-term proliferation of primary acute myeloid leukemia blasts under liquid culture conditions.

A. Schematic visualization of the JNJ-75276617 inhibitor drug screen in primary AML patient samples. B. Schematic overview showing gating strategy of the menin-KMT2A inhibitor drug screen. C. Dose-dependent effects on cell viability upon treatment of primary AML samples with JNJ-75276617 under liquid culture conditions. Statistical analysis by unpaired Student's t test. * $P < 0.05$, ** $P < 0.01$, *** $P < 0.001$.

Supplemental figure 2. JNJ-75276617 impairs long-term proliferation of primary acute myeloid leukemia blasts under MS5 coculture conditions.

Dose-dependent effects on cell viability upon treatment of primary AML samples with JNJ-75276617 under MS5 co-culture conditions. Statistical analysis was performed by by an unpaired Student's t test. * $P < 0.05$, ** $P < 0.01$, *** $P < 0.001$.

Supplemental figure 3. Effects of JNJ-75276617 on long-term proliferation in distinct genetic acute myeloid leukemia subgroups.

A. Boxplots showing AUC values of the proliferation of *NPM1c*, *DNMT3A*, *FLT3*, *RUNX1*, *IDH1*, *TET2* and *CEBPA* mutant vs wild type samples on LQ day 7 and 14 and MS5 day 7 and 14. B. Heatmap of AUC values at day 7 for liquid (LQ) culture conditions and MS5 coculture conditions in primary AML patient samples with various mutations. Heatmap showing expression of CD11b normalized to control after treatment with JNJ-75276617 for LQ and MS5 culturing conditions. C. Paired analysis

of AUC values calculated for the effect of JNJ-75276617 inhibitor treatment on liquid (LQ) and MS5 co-cultured primary AML patient cells on day 7 and 14 (n=14, biological replicates day 7 and n=15, biological replicates day 14). D. Correlation plot comparing AUC values from MS5 day 7 and LQ day 7 (n=14). Statistical analysis by unpaired Student's t test or Simple Linear Regression. * P < 0.05, ** P < 0.01, *** P < 0.001.

Supplemental figure 4. JNJ-75276617 drives differentiation of primary acute myeloid leukemia blasts.

A. Lineplots showing the MFI of CD11b normalized to the DMSO control for LQ day 7 (n=12). Black curves represent samples in which JNJ-75276617 also blocked proliferation, red curves represent samples in which proliferation was less effected by JNJ-75276617 treatment. B. Comparison between AUC and CD11b expression (normalized to DMSO control) identifying 4 groups: proliferation, differentiation and proliferation, differentiation only, and weak responders. Red dots represent samples in which proliferation was less effected by menin-KMT2A inhibition. C. Barplots depicting the MFI of CD11b (normalized to DMSO control) of CB KMT2A-AF9 on LQ day 7. D. Cytospins of DMSO and 3.0 µM JNJ-75276617 inhibitor treated CB KMT2A-AF9 cells at LQ day 7. E. Boxplots showing AUC values of the normalized MFI of CD11b of *NPM1c*, *DNMT3A*, *FLT3*, *RUNX1*, *TET2, CEBPA* and KMT2A-rearr. mutant vs wild type on LQ day 7 and 14 and MS5 day 7 and 14. NA = not assessed due to little number of samples in testing conditions. Statistical analysis by unpaired Student's t test. * P < 0.05, ** P < 0.01, ** P < 0.001.

Supplemental figure 5. Quantitative proteome analyses links menin-KMT2A inhibitor sensitivity to more committed L-GMP-type acute myeloid leukemias in *NPM1*^{wt} only

A. Volcano plot of the pearson correlation coefficient and log10 p-values of proteome dataset versus AUC values of LQ day 7. B. Dotplot of gene set enrichment analysis (GSEA) signatures enriched in sensitive and less sensitive primary AML samples at LQ day 7. C. Highlighted gene set enrichment signatures from panel B. D. Volcano plot of the pearson correlation coefficient and log10 p-values of proteome dataset versus AUC values of MS5 day 7. E. Highlighted gene set enrichment signatures from panel B. F. Protein expression of HOXA10 and MEIS1 in *NPM1*^{wt} and *NPM1c* AML samples. Red dots and annotated samples are *NPM1*^{wt} AMLs sensitive to menin-KMT2A inhibition.

Supplemental figure 6. Quantitative proteome analyses links menin-KMT2A inhibitor sensitivity to more committed L-GMP-type acute myeloid leukemias in *NPM1*^{wt} only

A. Comparison between AUC and HOXA10, MEIS1, or IGF2BP2 protein expression in primary AML samples cultured for 7 days under liquid conditions. Red dots *NPM1c*, black dots *NPM1*^{wt}. Annotated samples are *NPM1*^{wt} AMLs sensitive to menin-KMT2A inhibition. B. Comparison between AUC and HOXA10, MEIS1, or IGF2BP2 protein expression in primary AML samples cultured for 7 days under liquid conditions. Red dots annotate *NPM1c*, black dots *NPM1*^{wt}. C. Dotplots showing GSEA signatures enriched in sensitive and less sensitive *NPM1*^{wt} only AMLs. D. Comparison between AUC values in GMP-like, Mixed and HSC-like groups of LQ day 7. E. Dotplot showing GSEA signatures enriched in NPM1c/DNMT3Amut AML samples from the TCGA

dataset. F. Dotplot showing GSEA signatures enriched in NPM1c/DNMT3Amut AML samples from the proteome dataset. Statistical analysis by unpaired Student's t test. * P < 0.05, ** P < 0.01, ** P < 0.001.

Supplemental figure 7. HOXA9 expression upon menin-KMT2A inhibition

A. Barplots showing relative mRNA expression of *MEIS1, IGF2BP2 and HOXA9* in four-day JNJ-75276617 inhibitor-treated primary AML patient samples normalized to DMSO of AML36. Heatmap showing effect on proliferation (AUC) and induction of CD11b expression (normalized to DMSO control). B. Barplots showing relative mRNA expression of *MEIS1* and *IGF2BP2* in four-day JNJ-75276617 inhibitor-treated OCI-AML3 and MOLM13 cells normalized to DMSO. C. Barplots depicting absolute cell counts in OCI-AML3 and MOLM13 cells with EV-GFP or MEIS1-GFP treated with DMSO or 0.3 µM JNJ-75276617 inhibitor (representative of n=3). D. Relative mRNA expression of *IGF2BP2* in four-day JNJ-75276617 inhibitor-treated OCI AML3 cells with EV-GFP or IGF2BP2-GFP. E. Fold change DAPIneg/GFP+ counts of OCI-AML3 cells with EV-GFP or IGF2BP2-GFP treated with DMSO, 0.03, 0.3 or 3.0 µM JNJ-75276617 inhibitor for seven days. F. Relative mRNA expression of *MEIS1* and *BMI1* in four-day JNJ-75276617 inhibitor-treated OCI AML3 cells with EV-GFP or IGF2BP2-GFP. Error bars represent mean ± standard error of the mean (SEM). Statistical analysis by unpaired Student's t test or Simple Linear Regression. * P < 0.05, ** P < 0.01, *** P < 0.001.

Supplemental figure 8. GO analyses of loci with altered H3K4me3 marks.

A. GSEA signatures of a ranked fold change list of H3K4me3 expression changes after menin-KMT2A inhibition of AML2, AML22 and AML5. Processes associated with H3K4me3 downregulation are shown. B, GSEA as in A, but now processes associated

with H3K4me3 upregulation are shown. C. Dotplots showing gene ontology (GO) terms of genes with a fold change (FC)<-0.585 in H3K4me3 marks after treatment. D. As in C, but now dotplots for GO terms for genes with a FC>0.585 in H3K4me3 marks are shown.

Supplemental figure 9. GO analyses of loci with altered H3K4me3 and H3K27ac marks.

A. GSEA signatures of a ranked fold change list of H3K27ac expression changes after menin-KMT2A inhibition of AML2, AML22 and AML5. Processes associated with H3K27ac upregulation are shown. B. Dotplot of gene ontology (GO) terms of genes that have upregulated H3K4me3 expression in OCI-AML3 cells after JNJ-75276617 inhibitor treatment. FC > 0.585.

Supplemental figure 10. Menin-KMT2A inhibition drives HLA expression in a MEIS1-independent but CIITA-dependent manner in the case of MHC-II.

A. Relative mRNA expression of *HLA-A, HLA-DR and CIITA* in four-day JNJ-75276617 inhibitor-treated primary AML patient samples normalized to DMSO of AML36 or AML37 (*HLA-A*). Heatmap showing effect on proliferation (AUC) and induction of CD11b expression (normalized to DMSO control). B. Relative mRNA expression of *HLA-A, HLA-DR and CIITA* in four-day JNJ-75276617 inhibitor-treated primary AML patient samples normalized to DMSO of AML36 or AML37 (*HLA-A*). Samples not ranked based on AUC value. C. Correlation plots comparing fold changes of *HLA-DR* and *CIITA* mRNA expression after menin-KMT2A inhibition. D. Correlation plots comparing fold changes of *HLA-DR* and *MEIS1* mRNA expression after menin-KMT2A inhibition. E. Barplot showing MFI of HLA-DR expression in MV4-11 cells with EV-GFP

or MEIS1-GFP treated for four days with DMSO or JNJ-75276617 inhibitor (n=3). Statistical analysis by unpaired Student's t test. * P < 0.05, ** P < 0.01, *** P < 0.001.

Supplemental figure 11. Menin inhibition enhances T cell cytotoxicity

A. Barplots showing relative viable cell counts from the experiment shown in Figure 7C, determined by Annexin-V and Zombie NIR™, of 8 primary AML samples grown in the absence (0:1) or in the presence (5:1) of allogeneic T cells, whereby cell were pre-treated with DMSO or 0.3 µM JNJ-75276617. B. Primary AML samples were treated for four days with JNJ-75276617 or DMSO controls after which allogeneic T cells were added for an additional 3 days. Viable T cell counts are shown. C. $CD4^+$ percentage in viable T cells of primary AML sample cultures with T cells (enriched). D. Relative CD69 MFI expression in viable T cells from primary AML sample cultures without T cells (depleted) or with T cells (enriched). Statistical analysis by unpaired Student's t test. * P < 0.05, ** P < 0.01, ** P < 0.001.

Supplemental Methods

Primary samples

AML blasts from peripheral blood or bone marrow from untreated patients were studied after informed consent and the protocol was approved by the Medical Ethical Committee of the University Medical Center Groningen, The Netherlands, in accordance with the Declaration of Helsinki. Mononuclear cells (MNCs) were isolated via Lymphoprep™ separation and cryopreserved. Next Generation Sequencing was performed to obtain mutation status of primary AML cells using the TruSight Myeloid Sequencing Panel (Illumina) or exome sequencing. Neonatal cord blood (CB) samples

were obtained from healthy full-term pregnancies at the obstetrics departments at the Martini Hospital and University Medical Center Groningen.

Cell culture

The AML cell lines OCI-AML2 (DSMZ: ACC-99) and OCI-AML3 (DSMZ: ACC-582) were cultured in alpha MEM (Lonza). Cell line KG1A (DSZM: ACC-421) was cultured in IMDM (Lonza) and IMS-M2 cells were cultured in RPMI 1640 (Lonza) all with 20% fetal bovine serum (FCS, Sigma-Aldrich) and 1% penicillin/streptomycin (P/S, Gibco™). MV411 (DSMZ: ACC-102), MOLM13 (DSMZ: ACC-554), K562 (DSMZ: ACC-10), THP1 (DSMZ: ACC-16) and HL60 (DSMZ: ACC-3) cells were cultured in RPMI 1640 with 10% FCS and 1% P/S. CB MLL-AF9 cells[1] were cultured in Gartner's medium supplemented with IL-3 (Sandoz), SCF (Novus Biologicals) and FLT-3L (Amgen) (10 ng/ml each). MS5 murine stromal cells (DSMZ: ACC-441) were cultured in alpha-MEM (Lonza) with 10% FCS and 1% P/S. All cell cultures were kept at 37°C and 5% CO_2. For all menin-KMT2A interaction inhibition experiments inhibitor JNJ-75276617 was provided by Janssen Biologics BV.

Menin inhibitor screen in primary AML samples

Cryopreserved MNCs of AML patients were either cultured in liquid culture supplemented with G-CSF (Amgen), N-Plate (TPO)(Amgen) and IL-3 (Sandoz) (all 20 ng/mL) or co-cultured in Gartner's medium supplemented with cytokines on MS5, which were confluent plated on 0.1% gelatin-coated 48 wells plates and pre-treated with Mitomycin C. 150.000 MNCs per well were plated per well, and after two days recovery cells were treated with DMSO or 0.03, 0.30 and 3.00 µM JNJ-75276617 inhibitor for 14 days. Fresh medium and inhibitor were added at day 7 after demi-

population of the cells. On day 7 and 14 cells were stained with CD45-PECy7 (BioLegend; 304016), CD117-PE (ImmunoTools; 21271174X2), CD11b-FITC (ImmunoTools; 21279113X2), and DAPI (ThermoScientific) in a 96 wells plate, and were incubated for 30 min at 4°C. Fluorescence measurements were taken using a MACSQuant® X Flow Cytometer (Miltenyi Biotec)

Menin inhibitor screen in cell lines

AML cell lines were treated with DMSO or 0.03, 0.30 and 3.00 µM JNJ-75276617 inhibitor for 14 days. Every 2 days fresh medium and menin inhibitor was added after demi-population of the cells.. On day 7 and 14 cells were stained with DAPI in a 96 wells plate and analysed using a MACSQuant® X Flow Cytometer.

Menin inhibitor screen in healthy samples

Healthy MNCs were isolated from CB by a density gradient using Lymphoprep™ (STEMCELL™ Technologies). Stem cells were isolated using the CD34 Microbead Kit (Miltenyi). After 24h recovery in Stemline® II hematopoietic medium (Merck; #S0192) supplemented with 1% P/S, SCF, FLT3-L and N-plate (TPO)(Amgen)(all 100 ng/mL), $CD34^+$ CB cells were treated with DMSO or 0.03, 0.30 and 3.00 µM JNJ-75276617 inhibitor for 14 days in liquid culture with G-CSF (Amgen), N-Plate and IL-3 (all 20 ng/mL) or co-cultured on MS5 in Gartner's medium without supplementation of cytokines.

Flow cytometry data analysis inhibitor screen

All flow data was analysed using Flow Jo™ (BD BioSciences). Counts, percentages and Median Fluorescent Intensities were exported for further analysis. To calculate

area under the curve (AUC) values $DAPI^-/CD45^{dim}$ (primary samples) or $DAPI^-$ (cell lines) counts were normalized to the DMSO control. Next, AUC was calculated using trapezoid rule integration computed by the trapz() function in the R package caTools. CD11b MFI values were normalized to DMSO control.

Sample preparation and mass spectrometry analysis

Cryopreserved primary AML patient samples were thawed as described in the 'Menin inhibitor screen in primary AML samples' section. After thawing MNCs were isolated for $CD34^+$ (*NPM1*^{wt}), $CD117^+$ (*NPM1*^{cyt}) or depleted for CD3 (samples with low CD34/CD117%; CD3 MicroBeads, human; Mitenyi Biotec) by autoMACS (Miltenyi Biotec). 1.5E6 cells were snap frozen in liquid nitrogen. In addition, three peripheral blood $CD34^+$ healthy control samples were taken along as well.

Mass spectrometry analysis

Cell lysis and MS sample preparation for DIA SingleShot analysis

Cell lysis was performed in PreOmics LYSE buffer and samples were incubated at 95°C for 10 minutes.[2] Cell extracts were sonicated and protein concentrations were determined using a BCA protein assay. Complete cell extracts were digested employing 50 µl of PreOmics DIGEST reagent at 37°C overnight. Tryptic peptides were desalted by solid phase extraction using PreOmics CARTRIDGE according to the manufacturer's instructions. After lyophilization and resuspension in 0.1% formic acid, 1.7 µg of peptide per samples were applied to mass spectrometry analysis.

MS sample preparation for DDA Peptide Library generation

10 µg peptide of each sample (except of samples H1603 and H1604) were pooled and lyophilized. The pooled peptide sample was then subjected to pre-fractionation by high pH reversed phase chromatography[2] for deep proteome profiling. Briefly, peptides were reconstituted in 10 mM ammonium formate (pH 10, buffer A) and loaded onto an XBridge C18, 200 × 4.6 mm analytical column (Waters) operated with an UltiMate 3000 HPLC and UHPLC Systems (Thermo Fisher). Peptides were separated by applying a segmented gradient with increasing acetonitrile concentration from 7% to 30% buffer B (buffer A supplemented with 80% acetonitrile) over 15 min followed by a 5 min gradient to 55% buffer B. The collected fractions were combined in a concatenated way to generate a total of 10 fractions. Pooled fractions were then desalted via 100 mg SepPack C18 columns (Waters), lyophilized and reconstituted in 0.1% formic acid. For subsequent MS analysis, 1.7 µg of peptide per fractionated samples were applied in triplicates.

Mass spectrometric analysis

LC-MS/MS experiments were performed on a Q Exactive HF mass spectrometer (Thermo Fisher Scientific) equipped with an Easy nLC-1200 UPLC system (Thermo Fischer Scientific). Samples were loaded with an auto sampler onto a 40 cm fused silica emitter (New Objective) packed in-house with reversed phase material (Reprusil-Pur C18-AQ, 1.9 µm, Dr. Maisch GmbH) at a maximum pressure of 1150 bar. The bound peptides were eluted over 125 min run time and sprayed directly into the mass spectrometer using a nano electrospray ion source (ProxeonBiosystems). For the analysis of single shot samples, the mass spectrometer was operated in the data independent mode (DIA). The DIA-MS method consisted of a survey scan at 120,000

resolution from 350 to 1650 m/z. DIA windows (ms/ms scans) were acquired at 30,000 resolution and the number of windows was set to achieve 4 data points per peak.
For the analysis of peptide library samples, the mass spectrometer mass spectrometer was operated in a data-dependent acquisition mode to automatically switch between full scans (resolution R=60.000) and the acquisition of HCD fragmentation spectra (MS/MS mode) of the ten most abundant peptide ions in the Orbitrap mass analyzer (resolution R=15.000).

Mass spectrometry data processing

All raw files acquired in this study were collectively processed with the Dia-NN software suite (version 1.7.10) for peptide/protein identification and quantification using a human Uniprot database (downloaded February 2020).[3] Default parameters were used. Furthermore, the precursors identified at a Q-value below 1% were used to infer protein groups with an adapted version of the ID Picker algorithm.[4] The corresponding protein group intensities were computed with an adapted version of the maxLFQ algorithm[5] taking all assigned precursors into account. In addition to the LFQ intensities, iBAQ values were computed using the summed mean raw precursor intensities per peptide and the number of all theoretical unique tryptic peptides per protein group.[6] Copy number estimates and protein concentrations were calculated with Perseus (v 1.6.0.2)[7] applying the proteomic ruler[8] approach on the iBAQ values. Over 15.000 proteins could be quantified (PXD030487).

LFQ proteome data analysis

Pearson correlations were performed using the calculated AUC and the LFQ proteome dataset. Only genes with a row max of > 50 were taken along in further analysis. Gene set enrichment analysis were performed using ranked pearson coefficient values.

Heatmap and one minus pearson correlation clustering of *NPM1c* differentially expressed proteins were generated using the Morpheus tool from clue.io.

ChIP-seq with spike-in and data analysis

ChIP experiment

Chromatin immunoprecipitation was performed as described previously.[9] OCI AML3 cells were treated with 0.3 µM menin-KMT2A interaction inhibitors for 7 days and after cross linking spiked with drosophila chromatin. Primary AML samples were treated with 0.3 µM or 0.03 µM JNJ-75276617 inhibitor for 5 days and after cross linking spiked with mouse chromatin. The following antibodies were used: anti-H3K4me3 (C15200152; Diagenode), anti-H3K27ac (C15410196; Diagenode), anti-H3K27me3 (C15410195; Diagenode) and IgG (i8141, Sigma). Sequencing libraries were generated using the KAPA Hyper Prep Kit (Roche Sequencing and Life Sciences) according to manufacturer's protocol and sequenced on an Illumina NextSeq500 using default parameters.

Alignment

ChIP-rx data analysis was done as described in Orlando *et al.*, 2014.[10] In short, combined reference genomes were generated for human (hg38) and drosophila (dm6) or human (hg38) and mouse (mm10) with 'dm6_' or 'mm10_' suffix to avoid chromosome name duplications. Obtained paired-end reads were aligned to the metagenomes using Burrows-Wheeler Aligner (BWA)[11] with default settings. Generated SAM files were split in two resulting in a file containing reads that aligned to human chromosomes and a file containing reads that aligned either to drosophila

chromosomes or mouse chromosomes. Aligned reads were further processed using SAMtools.[12] Normalization factors were calculated per file as described in Orlando *et al.*, 2014.[10]

Visualization of tracks

To visualize the tracks bigwig files were generated by determining the total number of overlapping fragments at each position in the genome using BEDtools genomecov. The coverage was scaled using the calculated normalization factors. Subsequently, BedGraph files were converted to BigWig files using UCSC bedGraphToBigWig. Tracks were visualized using the Integrative Genomics Viewer.[13] Data is deposited at GSE237834.

Peak calling and further processing

Peaks were called using MACS2[14] with estimated fragment size and broad settings. To be able to compare coverage from different samples peaks were concatenated and merged per histone mark. For every track read counts were generated and the coverage was normalized using the normalization factor calculated before.

Quantitative real-time PCR

RNA samples were prepared from cell lines and primary AML patient samples treated with DMSO or menin inhibitor for various timepoints. Total RNA was isolated using the RNeasy Mini Kit from Qiagen (Venlo, The Netherlands) according to the manufacturer's protocol and reverse transcribed using the iScript cDNA synthesis kit (Bio-Rad). Subsequently, the cDNA was amplified using SsoAdvanced SYBR Green

Table 2. Primers used for ChIP-qPCR		
Target	**Forward**	**Reverse**
CIITA -0.5	GAAAATGACAGGTGGGCCACTTATGATCTC	TCCCACACCAAATTGCCCTGAATTTCTC
CIITA -0.2	AACAGACTTTCTGTGCAACTTTCTGTCTTC	TGAACACCCTCTAATTTTACCACACTCCC
CIITA +1.7	TGCTTGGTTGCTCCACAGCCTG	CCCGCAGTTCTTTTTCCCTTTCACTTTC
HLA-DR -0.6	AAGCTCTTGGCCTGAGTTGA	CAGGCCATGGAGATTGTCTGA
HLA-DR -0.2	GTCTGTTCTGCCTCACTCCC	ATCCTAGCACAGGGACTCCA
HLA-DR +0.2	GGTGGAGTTCTTCCCTCACC	TGGCTTGTAGCAGGACCTTG

Supermix (Bio-Rad) on a CFX384 Touch Real-Time PCR Detection System (Bio-Rad). Primer sequences are listed in table 1 and 2.

Generation of MEIS1-EGFP, IGF2BP2-IRES-EGFP and EGFP-MEN1 lentivectors

Generation of lentiviral pRRL SFFV MEIS1-EGFP was done by Genscript. The EGFP-MEN1 expression vector was constructed by amplifying the MEN1 cDNA sequence and EGFP sequence from K562 derived cDNA and pEGFP-C1 (Takara Bio Europe SAS), respectively. The IGF2BP2-IRES-EGFP expression vector was constructed by amplifying IGF2BP2 cDNA sequence and EGFP sequence from THP1-derived cDNA and pEGFP-C1, respectively. For the EGFP-MENIN1 vector, primers were designed to have 5' overhangs complementary to the fusion partners and the amplified products was ligated using Gibson assembly in EcoRI/BsrGI-cut pRRL-SFFV-IRES-EGFP. For the IGF2BP2-IRES-EGFP vector, the same strategy was followed and the amplified product was ligated in XhoI-cut pRRL-SFFV-IRES-EGFP. The construct sequence was verified by Sanger sequencing.

Table 1. Primers used for mRNA expression		
Target	**Forward**	**Reverse**
MEIS1	TCTGCCACCGGTATATTAGC	GAACGAGTAGATGCCGTGTC
IGF2BP2	TTCGAAACATCCCTC	CTGTGTCTGTGTTGACTTGTT
HLA-A2	TCCTGCTACTCTCGGGGGCT	CTCCCACTTGTGCTTGGTGG
HLA-DRA	CTGAGGACGTTTACGACTG	CACACCACGTTCTCTGTAG
CIITA	GGCTGGGATTCCTACACA	ACACTGTGAGCTGCCTTG
BMI1	GTTCCCTCCACCTCTTCTTG	GGCTCTTGCTGGTTCCATTC

Generation of CRISPR/Cas9 knockout lines

3xNLS-SpCas9 expression and purification

Gene editing was essentially performed as we described previously.[15] 3xNLS-SpCas9 was purified essentially according to the method described in Wu et al, 2019[16] with some modifications. In short: the vector pET-21a_3xNLS-SpCas9 was obtained from Addgene (Addgene, #114365) and transformed to Rosetta 2(DE3)pLysS competent cells (Novagen, Merck, Amsterdam, the Netherlands). One single colony was precultured overnight at 37 °C in 10 ml of LB medium containing Ampicillin (100 µg/ml) and Chloramphenicol (34 µg/ml) and subsequently diluted in 1 liter of TB medium containing Ampicillin, Chloramphenicol and 0,5 mM IPTG and grown overnight (16 hours) at room temperature with vigorously shaking. The next day, the culture was harvested, centrifuged for 20 minutes at 3000 g and the pellet was resuspended in 20 ml of Ni-NTA binding buffer (20 mM TRIS, 500 mM NaCl, 20 mM imidazole, 1 mM TCEP, pH 8.0), flash frozen in liquid nitrogen and stored at -20 °C.

For purification, the bacterial suspension was thawed and PMSF (1 mM final concentration) and lysozyme (final concentration of 0,5 mg/ml) was added and incubated at room temperature for 10 minutes with rotation. DNAse (Roche, Merck, Amsterdam, the Netherlands) was added (0,01 mg/ml final concentration) and the solution was incubated with rotation for another 30 minutes at room temperature. The lysate was cleared by centrifugation for 30 minutes at 20.000 g, 3 ml Ni-NTA agarose slurry (Qiagen, Venlo, the Netherlands) was added to the supernatant and rotated for 1 hour at 4 °C. The Ni-NTA bead containing lysate was divided over 3 Polyprep columns (Bio-Rad, Veenendaal, the Netherlands) and after settling the column, the beads were washed 2 times with 5 ml of Ni-NTA binding buffer. The protein was eluted

with 1,3 ml elution buffer (20 mM TRIS, 250 mM NaCl, 250 mM Imidazole, pH 8.0) per column and pooled. The eluate was diluted 10 times with SCX wash buffer (50 mM HEPES, 400 mM NaCl2, pH 7,4) to decrease the imidazole concentration and loaded onto a 5 ml HiTrap SP FF strong cation exchange column (Cytivia, Merck, Amsterdam, the Netherlands) with a flow rate of 5 ml/min. The column was washed with 50 ml SCX wash buffer and the protein was eluted with SCX elution buffer (50 mM HEPES, 700 mM NaCl2, pH 7,4) while collecting fractions of 0,5 ml. The A280 of the fractions was measured and the fractions containing the purified protein were pooled (4,5 ml total) and desalted in 3 portions of 1,5 ml over a 5 ml HiTrap desalting column (Cytivia, Merck, Amsterdam, the Netherlands) equilibrated with storage buffer (20 mM HEPES, 150 mM NaCL2, 10% glycerol, pH 7,4). The resulting purified and desalted protein was concentrated to 1 ml using an Amicon Ultra 15, 100.000 MWCO spin filter (Millipore, Merck, Amsterdam, the Netherlands), the concentration was measured and adjusted to 5 mg/ml. 20 µl portions were flash frozen in liquid nitrogen and stored at -80 °C for further use.

Guide RNA selection

The online platform Benchling (www.benchling.com) was used to design guide RNA sequences for CIITA. Two different gRNAs were selected based on high on-target and off-target scores. gRNA sequences are listed in table 3.

sgRNA preparation

sgRNA was made by *in vitro* transcription of a dsDNA PCR product. In short: a DNA template was made by oligo assembly using a set of three generic oligos (Sp6-forward, scaffold oligo and Sp6-reverse) and one guide specific oligo. PhusionII HF polymerase

(Thermo Scientific, Bleiswijk, the Netherlands) was used to amplify the DNA template. Final PCR products have the following sequence: 5'-GATCATTTAGGTGACACTATA(G)NNNNNNNNNNNNNNNNNNNGTTTAAGAGCTATGCTGGAAACAGCATAGCAAGTTTAAATAAGGCTAGTCCGTTATCAACTTGAAAAAGTGGCACCGAGTCGGTGC-3', in which N stands for the specific guide sequence and (G) stands for the addition of an extra G when the guide sequence does not have a 5' G. The Sp6 priming sequence is underlined. The sequences of the oligos are listed in table 4. The template contains an Sp6 priming site to facilitate in vitro transcription using a HiScribe SP6 RNA synthesis kit (New England Biolabs, Ipswich, MA, USA). 300 ng template was used in an overnight reaction, which typically yielded 100-150 µg sgRNA. sgRNA was purified by a Monarch RNA cleanup kit (New England Biolabs, Ipswich, MA, USA) according to the manufacturer's instructions and stored at -80°C until use.

Procedure

RNP complexes were formed *in vitro* by adding 12 µg sgRNA to 20 µg spCas9 and incubation for 15 minutes at room temperature. MV4-11 cells (1 x106) were washed once with PBS and resuspended in 100 µl K562 electroporation buffer (88 mM KH2PO4, 14 mM NaHCO3, 12 mM MgCl2, 2 mM glucose and 6 mM ATP, pH 7,4), the RNP complex was added and transferred to a 2 mm gap width electroporation cuvette. The mixture was electroporated with an Amaxa I electroporation device (Lonza, Geleen, the Netherlands) using program D-23, immediately transferred to 4 ml fresh medium (RPMI1640 + 10 % FCS) and cultured for 3 days. Single cells were sorted in 96 well plates using a MoFlo XDP cell sorter (Beckman Coulter, woerden, the Netherlands) and incubated for 12 days whereafter plates were scored for the

presence of growing colonies. Approximately 12 clones per sgRNA were expanded in 24 well plates and gDNA was extracted from a part of the clone. gDNA spanning the expected cut site was PCR amplified using primers listed in table 5 and Sanger sequenced. Sequencing tracks were analyzed using the online available TIDE analysis tool (www.tide.nki.nl). Clones with lesions resulting in premature stop codons on both alleles were expanded and frozen. For experiments, clones were pooled again to avoid possible clonal differences unrelated to the knockouts.

Table 3: guide RNA targets			
Gene	**Guide**	**Exon**	**Target sequence**
CIITA	1	8	GAGATTCAGGCAGCTCAACG
	2	8	GAGCTGCCTGAATCTCCCTG

Table 4: sequences of the DNA template oligos for sgRNA production	
Oligo	Sequence
Sp6-forward	GATCATTTAGGTGACACTATAG
Scaffold oligo	GCACCGACTCGGTGCCACTTTTTCAAGTTGATAACGGACTAGCCTTATTTAAACTTGCTATGCTGTTTCCAGCATAGCTCTTAAAC
Sp6-reverse	GCACCGACTCGGTGCCAC
CIITA (1)	GATCATTTAGGTGACACTATAGAGATTCAGGCAGCTCAACGGTTTAAGAGCTATGCTGGAAAC
CIITA (2)	GATCATTTAGGTGACACTATAGAGCTGCCTGAATCTCCCTGGTTTAAGAGCTATGCTGGAAAC

Table 5: primers used for sequencing of CRISPR/Cas9 targets		
Target	Forward	Reverse
CIITA exon 8	TAAGGCAGGGACTGTCAGGAAC	TGCAAGGATGCACACCAAAC

Flow cytometry analysis

Hetero- and homozygous *CIITA* knockout MV4-11 cells were treated with 0.03, 0.30 or 3.00 µM JNJ-75276617 inhibitor for four days after which 100.000 cells were stained for HLA-DR-PE (Biolegend; 307606) and incubated for 30 min at 4°C. Fluorescence measurements were taken using a MACSQuant® X Flow Cytometer (Miltenyi Biotec).

Allogeneic and autologous killing assay

T-cell isolation and activation

Allogeneic T cells were isolated from cord blood or peripheral blood samples from healthy or allogeneic donors. MNCs were isolated by a density gradient using Lymphoprep™ (STEMCELL™ Technologies) and $5x10^6$ MNCs were plated into 6 well plates. Next, the non-adherent cells were collected and T-cells were isolated with the Pan T Cell Isolation Kit (Miltenyi Biotec) using the autoMACS (Miltenyi Biotec). To activate the isolated T-cells the cells were cultured in RPMI medium supplemented with 10% FCS, 1% P/S, IL-2 (6000 IU/ml) and Gibco Dynabeads Human T-Activator CD3/CD28 beads for 9 days. Autologous T cells were isolated from MNCs of primary AML patient samples using the Pan T Cell Isolation Kit as described above. After a 24h recovery these T-cells were activated for 3 days using IL-2 (6000 IU/ml) and Gibco Dynabeads Human T-Activator CD3/CD28 beads.

Preparation AML cells

MV411 and MOLM13 cells were cultured as described above and treated with 0.1 µM or 0.3 µM menin inhibitor for 4 days. Primary AML samples were thawed as described in section 'Menin inhibitor screen in primary AML samples' and cultured in α-MEM with 20% FCS and 1% P/S supplemented with G-CSF (Amgen), N-Plate (TPO)(Amgen) and IL-3 (Sandoz) (all 20 ng/mL). After one recovery day the cells were treated with 0.3 µM menin inhibitor for 4 days. After 4 days the cells were collected for T-cell killing and stained for HLA-DR-PE (Biolegend; 307606) after which they were incubated for 30 min at 4°C. Fluorescence measurements were taken using a MACSQuant® X Flow Cytometer (Miltenyi Biotec).

Allogeneic killing assay

To start the allogeneic killing assay, PBMCs and activated T-cells were washed with serum free medium and stained with CellTrace™ Violet Cell Proliferation dye (ThermoFisher) for 20 min at 37ºC. Next, the cells were washed twice with serum containing medium and effector to target cell ratios were determined. The immune cells were loaded on top of the AML cells and after 3 days cells were stained with a staining mix containing Ca2+ buffer (BD Biosciences), AnnexinV-APC (Biolegend), and Zombie NIR (Biolegend). All flow cytometry was done using the NovoCyte Quanteon Flow Cytometer Systems 4 Lasers (Agilent).

Autologous killing assay

60.000 $CD3^+$-depleted primary AML cells were seeded with or without 10.000 autologous T cells (T-enriched or T-depleted, respectively) in RPMI with 10% FCS and 1% P/S. Cells were then treated with DMSO (WAK-Chemie Medical GmbH) or JNJ-75276617 0.3 µM for 4 days. Afterwards, the cells were stained with a staining mix containing Ca2+ buffer (BD Biosciences), AnnexinV-APC (Biolegend; 640941), Zombie NIR (Biolegend; 423106), CD3-BV785 (Biolegend; 317330) and CD45-PE (Biolegend; 304008). Simultaneously, 100.000 cells were stained for HLA-A,B,C-APC (Biolegend; 311410) and HLA-DR,DP,DQ-FITC (Biolegend; 361706). All flow cytometry measurements were done using the NovoCyte Quanteon Flow Cytometer Systems 4 Lasers (Agilent).

Data analysis allogeneic and autologous killing

All flow data were analyzed with NovoExpress Software (Agilent). After excluding immune cells based on cell trace violet, viable AML cells were gated out by AnnexinV-

APC and Zombie NIR. Counts were exported for further analysis. Fold change was calculated by normalizing all other treatments to their own controls, namely 0:1 E:T ratio, DMSO-treated cells and DMSO-treated T-depleted conditions in cell line killing, primary AML allogeneic killing, and primary AML autologous killing respectively.

Statistics

All statistical analyses were performed using the student t test paired or unpaired and were expressed as means ± SEM for all other comparisons. Differences were considered statistically significant at $p \leq 0.05$.

References

1. Horton SJ, Jaques J, Woolthuis C, et al. MLL-AF9-mediated immortalization of human hematopoietic cells along different lineages changes during ontogeny. *Leukemia*. 2013;27(5):1116–26.
2. Kulak NA, Pichler G, Paron I, Nagaraj N, Mann M. Minimal, encapsulated proteomic-sample processing applied to copy-number estimation in eukaryotic cells. *Nat Methods*. 2014;11(3):319–24.
3. Demichev V, Messner CB, Vernardis SI, Lilley KS, Ralser M. DIA-NN: neural networks and interference correction enable deep proteome coverage in high throughput. *Nat Methods*. 2020;17(1):41–44.
4. Ma Z-Q, Dasari S, Chambers MC, et al. IDPicker 2.0: Improved protein assembly with high discrimination peptide identification filtering. *J Proteome Res*. 2009;8(8):3872–81.
5. Hein MY, Hubner NC, Poser I, et al. A human interactome in three quantitative dimensions organized by stoichiometries and abundances. *Cell*. 2015;163(3):712–723.
6. Schwanhäusser B, Busse D, Li N, et al. Global quantification of mammalian gene expression control. *Nature*. 2011;473(7347):337–342.
7. Tyanova S, Temu T, Sinitcyn P, et al. The Perseus computational platform for comprehensive analysis of (prote)omics data. *Nat Methods*. 2016;13(9):731–40.

8. Wiśniewski JR, Hein MY, Cox J, Mann M. A “proteomic ruler” for protein copy number and concentration estimation without spike-in standards. *Mol Cell Proteomics*. 2014;13(12):3497–506.

9. Frank SR, Schroeder M, Fernandez P, Taubert S, Amati B. Binding of c-Myc to chromatin mediates mitogen-induced acetylation of histone H4 and gene activation. *Genes Dev*. 2001;15(16):2069–82.

10. Orlando DA, Chen MW, Brown VE, et al. Quantitative ChIP-Seq normalization reveals global modulation of the epigenome. *Cell Rep*. 2014;9(3):1163–70.

11. Li H, Durbin R. Fast and accurate short read alignment with Burrows-Wheeler transform. *Bioinformatics*. 2009;25(14):1754–1760.

12. Li H, Handsaker B, Wysoker A, et al. The Sequence Alignment/Map format and SAMtools. *Bioinformatics*. 2009;25(16):2078–2079.

13. Robinson JT, Thorvaldsdóttir H, Winckler W, et al. Integrative genomics viewer. *Nat Biotechnol*. 2011;29(1):24–6.

14. Zhang Y, Liu T, Meyer CA, et al. Model-based analysis of ChIP-Seq (MACS). *Genome Biol*. 2008;9(9):R137.

15. Cunningham A, Erdem A, Alshamleh I, et al. Dietary methionine starvation impairs acute myeloid leukemia progression. *Blood*. 2022;140(19):2037–2052.

16. Wu Y, Zeng J, Roscoe BP, et al. Highly efficient therapeutic gene editing of human hematopoietic stem cells. *Nat Med*. 2019;25(5):776–783.